

JGR Atmospheres

RESEARCH ARTICLE

10.1029/2021JD035296

Key Points:

- An extensive set of primary emissions and secondary photochemical products was measured in a remote location in the Yellow River Delta
- Elevated levels of anthropogenic volatile organic compounds (VOCs) and their oxidation products such as O₃ and peroxyacyl nitrates (PANs) indicate the impacts of urban and Oil and Natural Gas (O&NG) emissions
- Photochemistry in the Yellow River Delta is investigated in detail using in situ chemical measurements and 0-D box model simulations

Supporting Information:

Supporting Information may be found in the online version of this article.

Correspondence to:

L. G. Huey,
greg.huey@eas.gatech.edu

Citation:

Lee, Y., Huey, L. G., Wang, Y., Qu, H., Zhang, R., Ji, Y., et al. (2021). Photochemistry of volatile organic compounds in the Yellow River Delta, China: Formation of O₃ and peroxyacyl nitrates. *Journal of Geophysical Research: Atmospheres*, 126, e2021JD035296. <https://doi.org/10.1029/2021JD035296>

Received 24 MAY 2021

Accepted 15 OCT 2021

Author Contributions:

Conceptualization: L. G. Huey, Y. Wang, X. Wang

Data curation: Y. Lee

Formal analysis: Y. Lee, H. Qu

Funding acquisition: L. G. Huey, Y. Wang

Investigation: Y. Lee, L. G. Huey, Y. Wang, R. Zhang, Y. Ji, D. J. Tanner, X. Wang, W. Song, W. Hu

Methodology: Y. Lee, L. G. Huey, H. Qu, R. Zhang, D. J. Tanner

Project Administration: Y. Wang, X. Wang

Supervision: L. G. Huey

Writing – original draft: Y. Lee

Photochemistry of Volatile Organic Compounds in the Yellow River Delta, China: Formation of O₃ and Peroxyacyl Nitrates

Y. Lee¹, L. G. Huey¹ , Y. Wang¹ , H. Qu^{1,2} , R. Zhang^{1,3} , Y. Ji¹, D. J. Tanner¹, X. Wang⁴ , J. Tang⁵ , W. Song⁴ , W. Hu⁴ , and Y. Zhang⁴ 

¹School of Earth and Atmospheric Sciences, Georgia Institute of Technology, Atlanta, GA, USA, ²Now at Georgia Department of Natural Resources, Environmental Protection Division, Atlanta, GA, USA, ³Now at Microsoft Corporation, Redmond, WA, USA, ⁴State Key Laboratory of Organic Geochemistry, Guangzhou Institute of Geochemistry, Chinese Academy of Sciences, Guangzhou, China, ⁵CAS Key Laboratory of Coastal Environmental Processes and Ecological Remediation, Yantai Institute of Coastal Zone Research, Chinese Academy of Sciences, Yantai, China

Abstract An extensive set of primary and secondary pollutants was measured at a ground site in a remote location in the Yellow River Delta, China during the Ozone Photochemistry and Export from China Experiment (OPECE) from March to April 2018. The measurements include volatile organic compounds (VOCs), peroxyacyl nitrates (PANs), ozone (O₃), particulate species, nitrogen oxides (NO_x), and SO₂. Observed VOC mixing ratios were comparable to those measured in heavily polluted cities in the U.S. and China. The VOC source signatures suggest a strong influence from Oil and Natural Gas (O&NG) emissions with potentially large contributions from Liquefied Petroleum Gas (LPG) sources as well. Consistently elevated concentrations of O₃, PAN, and its rarely measured homologs peroxybenzoylic nitric anhydride (PBzN) and peroxyacrylic nitric anhydride (APAN) at the OPECE site indicate complex photochemistry in a heterogeneous VOC environment. Diagnostic 0-D box model simulations are used to investigate the budgets of RO_x (OH + HO₂ + RO₂), and the rate and efficiency of O₃ production. Model sensitivity calculations indicate that O₃ production at OPECE site is VOC limited in spring. This suggests that reduction in VOCs should be a priority for reducing O₃, where production and fugitive emissions from O&NG provide an attractive target. While initial reductions in NO_x might increase O₃ production, reduction of NO_x along with VOCs will be a necessary step to achieve long-term ozone reduction.

Plain Language Summary We observed the trace gas composition of the lower atmosphere in a remote location in the Yellow River Delta (YRD), China. The composition and source signatures of VOCs suggest a strong influence of Oil and Natural Gas (O&NG) emissions as well as urban emissions. Elevated levels of secondary pollutants such as O₃ and PANs indicate significant photochemical processing of volatile organic compounds (VOCs) and NO_x. Both measurements and diagnostic model simulations suggest that reduction in anthropogenic VOCs is a necessary step to reduce O₃ in the YRD region in spring, where O&NG and petrochemical facilities are important sources of such VOCs.

1. Introduction

Emission of volatile organic compounds (VOCs) to the atmosphere and their subsequent photochemical reactions involving nitrogen oxides (NO + NO₂ = NO_x) forms secondary pollutants such as ozone, peroxyacyl nitrates, and particulate matter (Seinfeld & Pandis, 2016). Rapidly growing sources of VOCs and NO_x in the U.S. and other countries are process and fugitive emissions from oil and natural gas (O&NG) extraction and use (Duncan et al., 2016). O&NG emissions can have a large impact on atmospheric composition and air quality on local to regional scales. Previous studies in the U.S. have demonstrated that activities associated with O&NG production (e.g., drilling, production, transport, and gas flaring) and oil and gas leakage from active and abandoned wells are significant sources of VOCs such as methane (CH₄), nonmethane hydrocarbons (NMHCs), and NO_x (Dix et al., 2020; Gilman et al., 2013; Helmig, 2020; Pètron et al., 2012; Warneke et al., 2014). For example, significantly elevated levels of C₂–C₅ alkanes were observed at 200–300 times above the regional and seasonal background in the Uintah Basin, Utah, which resulted in elevated O₃ levels (>150 ppbv) during a strong temperature inversion in the winter (Edwards et al., 2013; Helmig et al., 2014; Warneke et al., 2014). High levels of anthropogenic VOCs, primarily a range of light alkanes and aromatics, from O&NG sources were observed both in near-surface air and aloft over the Colorado Northern Front Range

Writing – review & editing: L. G. Huey, Y. Wang, H. Qu, R. Zhang, Y. Ji, D. J. Tanner, X. Wang

(NFR) (Brown et al., 2013; Peischl et al., 2018; Pètron et al., 2014). The evolution of plumes emanating from O&NG sources produce elevated levels of O₃, peroxyacyl nitrates (PANs), and organic aerosols (OA) in the NFR and the Denver urban area (Bahreini et al., 2018; Bien & Helmig, 2018; Lindaas et al., 2019; McDuffie et al., 2016; Swarthout et al., 2013; Zaragoza et al., 2017). Extensive field measurements in the Houston Ship Channel during the Texas Air Quality Study (TexAQS) 2000 and 2006 campaigns demonstrated that primary emissions such as reactive alkenes (e.g., ethene and propene) and its downwind evolution were a primary contributor to severe O₃ exceedances in the Houston metropolitan area (Gilman et al., 2009; Ryerson et al., 2003; Washenfelder et al., 2010; Zhou et al., 2014).

In parallel with rapid industrialization over the past few decades, China has become the world's second-largest consumer of oil behind the United States (EIA, 2020). The growth of China's oil consumption has led to the rapid development and expansion of oil and natural gas fields with production of 4.9 million barrels of petroleum and other liquids per day in 2019 (EIA, 2020). Major O&NG fields such as the Daqing and Shengli fields are located in the Songliao Basin and Bohai Bay Basin, respectively, on the North China Plain (NCP). This region has experienced severe air pollution problems (Li et al., 2017; Qu et al., 2020; Wang et al., 2017), and mitigation is a challenge due to uncertainties in complex source characteristics and photochemistry in markedly polluted environments (e.g., Ma et al., 2019; Le et al., 2020; Qiu et al., 2020). For example, increasing trends in ozone levels have been observed in contrast with continuous reductions in NO_x emissions and particulate matter over the NCP (Gu et al., 2013; Li, Jacob, et al., 2019; Li et al., 2020). A few studies have looked at the effect of these O&NG emission sources on air quality in the NCP, focusing on VOC composition and ozone production (Chen et al., 2020). Despite the important impacts of the emissions from O&NG activities, field measurements in the O&NG regions in China are still scarce.

The Yellow River Delta Ecology Research Station of Coastal Wetlands (YRD), considered here, is located in a remote coastal location in Shandong province. Eastern Shandong province has the largest concentration of petrochemical refineries as well as active O&NG extraction sites in China. The station is near the Shengli field which is the second-largest producer of oil and natural gas in China, producing about 557,000 barrels/day of crude oil during 2014 (EIA, 2015). In addition to the O&NG emissions, the site can be influenced by the transport from upwind urban emissions in the NCP (e.g., Beijing, Tianjin, and Jinan), which typically have enhanced aromatics such as benzene and toluene characteristic of fossil-fuel combustion largely from mobile vehicles and industrial facilities (Li, Hao, et al., 2019; Zhang et al., 2016). Emissions of aromatics in East Asian Megacities have been identified as an important contributor to O₃ and aerosol production (e.g., Liu et al., 2012; Nault et al., 2018; Schroeder et al., 2020). However, model simulations of relatively simple compounds such as O₃ and PAN in China have often been biased low even with the addition of aromatics, suggesting missing VOC precursors (Fischer et al., 2014; Fu et al., 2007; Liu et al., 2010).

Sampling of relatively fresh emissions from O&NG and urban emissions and their secondary photochemical products including non-methane VOCs (NMVOCs), O₃ and reactive nitrogen (e.g., NO_x, PANs, and particulate nitrates) can be particularly important in an outflow region such as the YRD in China during springtime (Jacob et al., 2003; Talbot et al., 2003; Wang et al., 2006). Long-range pollutant transport from China can influence ozone concentrations, both in episodic increases and elevating regional backgrounds, in neighboring countries (e.g., Korea and Japan), the North Pacific Ocean and western North America. A large body of observations have accumulated in these regions to understand the impact of East Asian outflow. However, key uncertainties, including emissions and evolution of VOCs and NO_x, still remain due to a lack of relevant observations in the outflow regions in China. Thus, in situ chemical measurements in YRD provide a valuable data set which can be utilized to evaluate satellite observations and model simulations of this region.

In this paper, we report observations of the trace gas composition in a remote location in the Yellow River Delta downwind from O&NG and urban emissions during the Ozone Photochemistry and Export from China Experiment (OPECE) campaign. We report ground-based measurements of primary emissions and secondary photochemical products including CO, sulfur dioxide, nitrogen oxides, HONO (nitrous acid), VOCs, O₃, PAN, organic aerosols, and particulate nitrates. The mixing ratios of VOCs and reactivity toward the OH radical (i.e., OH reactivity) are compared with previous studies conducted in urban and O&NG producing region in the U.S. and China. We examine the daytime chemical removal of hydrocarbons from their diurnal variations and ratios of hydrocarbons as a function of OH exposure. In addition, we investigate the absolute

and relative abundance of PAN and its homologs (PANs) to characterize the photochemistry leading to reactive nitrogen processing. In addition, a near-explicit 0-D chemical box model with a comprehensive suite of observational constraints was utilized to estimate the budgets of RO_x ($OH + HO_2 + RO_2$) and the rate and efficiency of O_3 production. We evaluate local photochemistry of O_3 and reactive nitrogen using a case study based on in-situ observations and model simulations. Finally, we discuss implications of these findings for O_3 control strategies at the OPECE site.

2. Method

2.1. OPECE Campaign

The OPECE campaign was conducted in the Yellow River Delta Ecology Research Station of Coastal Wetland (YRD; 37°76'N, 118°98'E), from March 20 to April 21, 2018 (Figure 1a). This is a remote site located in a bird sanctuary in the Yellow River Delta (YRD). The closest urban area is Dongying which is 50 km to the southwest of the site. Larger urban areas, Ji'nan, Tianjin, and Beijing, are located to the southwest at about 200 km and to the northwest at about 200 and 300 km, respectively. Several active oil fields and petrochemical refineries including the Shengli O&NG field are located in the YRD region, where locations of O&NG emission sources in the region are described by Zhang, Sun, et al. (2019), Chen et al. (2020), and the China Energy Map by Rice University's Baker Institute (<https://www.bakerinstitute.org/chinas-oil-infrastructure>).

During the campaign, winds were primarily from the west and the ambient temperature varied from $-8^{\circ}C$ to $29^{\circ}C$ (Figure 1b). The site was consistently impacted by polluted air masses from both urban and O&NG emission sources. Relatively clean air, associated with high wind speeds from the south and southeast, was observed at the site on April 4–5, 2018. During this episode, substantially lower levels of VOCs (Figure S1 in Supporting Information S1) were observed along with the lowest levels of NO_x .

2.2. Ground-Based Instrumentation

In situ measurements were conducted with a large suite of instruments during the OPECE campaign. The physical layout of the instruments is shown in Figure 1a. The trace gas and particle measurements during the OPECE campaign are summarized in Table 1, along with methodologies, uncertainties, detection limits (LOD), sample intervals, and references. O_3 , NO_x , CO, and SO_2 were measured at 1 min resolution. The measurements of NO_2 were performed using a chemiluminescence (CL) NO_x monitor equipped with a molybdenum oxide converter, which is known to have a positive interference to NO_x oxidation products including HNO_3 , nitrous acid (HONO), PANs (peroxycarboxylic nitric anhydride), and organic nitrates (Winer et al., 1974). The NO_2 overestimation by CL NO_2 measurements in this work is likely biased by up to 20% based on the comparison of CL-based NO_2 instrument to other NO_2 measurement techniques in polluted environments such as Mexico City (Dunlea et al., 2007) and Beijing (Ge et al., 2013). For this reason, we assume an upper limit of 20% for this interference. The gas phase nitrous acid (HONO) was measured using a long path absorption photometer (LO-PAP), where the possible artifact of the LOPAP instrument is described in Kleffmann et al. (2006). A large set of alkanes, alkenes, aromatics, and oxygenated VOCs was measured using in situ gas chromatography with a flame ionization detector (GC-FID) and proton-transfer-reaction mass spectrometry (PTR-MS). PANs (RC(O)OONO₂) including peroxyacetic nitric anhydride (PAN), peroxypropionic nitric anhydride (PPN), peroxybutyric nitric anhydride (PBN), peroxyacrylic nitric anhydride (APAN), and peroxybenzoic nitric anhydride (PBzN) were measured by a thermal decomposition-chemical ionization mass spectrometry (TD-CIMS) method. Nitryl chloride (ClNO₂), molecular chlorine (Cl₂), dinitrogen pentoxide (N₂O₅), and formic acid (HC(O)OH) were measured by another chemical ionization mass spectrometers (CIMS). Measurements of inorganic and organic aerosol species were also conducted by a time of flight aerosol mass spectrometer (ToF-AMS). Meteorological parameters such as wind direction, wind speed, pressure, temperature, and relative humidity (RH) were obtained from the observatory of the Yantai Institute of Coastal Zone Research located near the OPECE site.

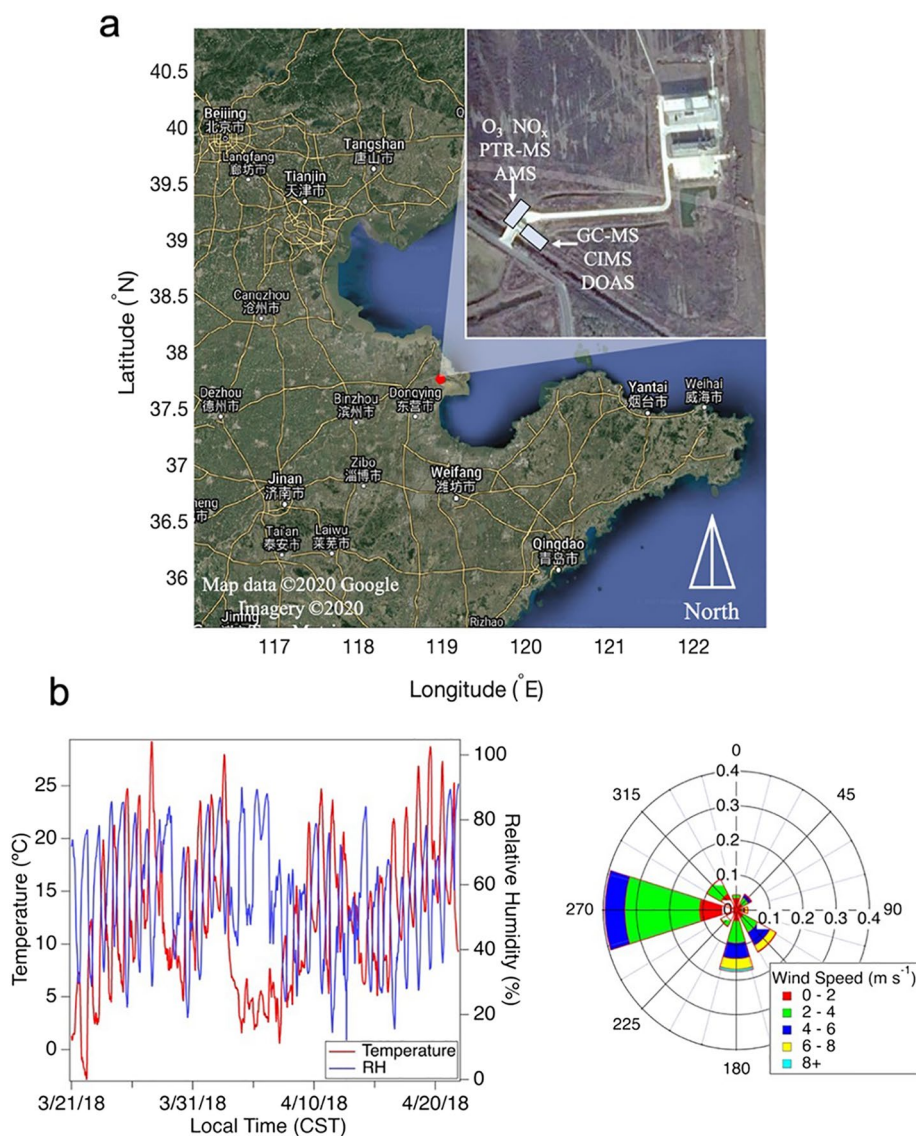


Figure 1. (a) Location of ozone photochemistry and export from China experiment (OPECE) site and surrounding provinces and major cities. The inset shows the physical layout of the ground-based instrumentation during the OPECE campaign. (b) Ambient temperature (red), relative humidity (blue) versus time in the left panel. The right panel is a wind rose plot.

2.3. Model Description

Detailed zero-dimensional model calculations utilize F0AM (The Framework for 0-D Atmospheric Modeling, Wolfe et al., 2016). The model incorporates the MCM v3.3.1 (Master Chemical Mechanism) to simulate radical budgets (i.e., OH, HO₂, and RO₂), O₃ production (PO₃), and production efficiency (OPE). All model constraints are averaged to a 10 min time step and include observations listed in Table S1 in Supporting Information S1. Measurements made with a time resolution longer than 10 min (e.g., NMHCs) were interpolated. Missing data points longer than two hours were replaced with their diurnal average. To account for variability in cloud cover and optical depth, the ratio of observed and MCM-calculated *J*-NO₂ is used to generate a correction factor that scales all *J*-values by the MCM parametrization (Wolfe et al., 2014). The scaling of *J*-values using the observed *J*-NO₂ is likely to be more uncertain for some *J*-values such as *J*-O¹D (Monks et al., 2004). The model was run to generate output for comparison with measurements made from March 20 to April 21, 2018, where observational constraints were updated every 10 min. A 30-day spin-up time is used to allow radicals and intermediate species

Table 1
Measurements During the OPECE Campaign

Measurement	Method	Uncertainty	LOD	Time resolution	Reference/Instrument
PANs	TD-CIMS using I ⁻ reagent ion	20%–30%	<7 pptv ^a	6 s	Slusher et al. (2004), Ji et al. (2020)
Cl ₂ , ClNO ₂ , N ₂ O ₅ , HC(O)OH	CIMS using I ⁻ reagent ion	30%	<6 pptv ^a	11 s	Liao et al. (2014), Ji et al. (2020)
CO	IR absorption	5%	40 ppbv	1 min	Thermo 48i
SO ₂	Pulsed fluorescence	10%	50 pptv	1 min	Thermo 43i
NO, NO ₂	Chemiluminescence	10%	50 pptv	1 min	Thermo 42i
O ₃	UV absorption	5%	1 ppbv	1 min	Thermo 49i
HONO	LOPAP	10%	3 pptv	1 min	Liu et al. (2019)/LOPAP-03 (QUMA, Germany)
NMHCs	GC-FID	22%	30–300 pptv	60 min	Lu et al. (2015)
	PTR-MS using H ₃ O ⁺ reagent ion	5%–30%	20–60 pptv	1 min	Wang et al. (2014b)/PTR-TOF 2000 (Ionicon Analytik GmbH, Austria)
Nonrefractory submicron aerosol ^b	ToF-AMS	30%	3–58 ng m ⁻³	2 min	DeCarlo et al. (2006)/AMS (Aerodyne Research Incorporated, USA)
Photolysis frequencies	Spectral radiometry	5%	1.5 × 10 ⁻⁶ s ⁻¹ /mV	1 min	Shetter and Müller (1999)/J-NO ₂ Filter Radiometer (Metcon, GmbH, Germany)

Note. GC-FID, gas chromatography with a flame ionization detector; LOD, detection limits; LOPAP, long path absorption photometer; PANs, peroxyacyl nitrates; TD-CIMS, thermal decomposition-chemical ionization mass spectrometry; ToF-AMS, time of flight aerosol mass spectrometer;

^aDetection limits are estimated from three times the standard deviation in background measurements. ^bMeasurements by aerosol mass spectrometer (AMS) include sulfate (SO₄²⁻), nitrate (NO₃⁻), ammonium (NH₄⁺), and organics.

to reach steady state. A first order loss is given to all species equivalent to a 24-hr lifetime. This is a dramatic simplification which prevents the buildup of longer-lived species, and helps account for the impact of advection, deposition, and dilution (e.g., Baier et al., 2017).

In addition to the full-campaign model run, a case study was formulated to investigate local photochemical formation of O₃ and PANs on April 6, 2018. For this period, average diurnal variations of O₃ and reactive intermediates show pronounced daytime formation observed after a clean episode (April 4–5, 2018) along with relatively slow wind speeds (~2 ms⁻¹) from April 5 through the early morning of April 6, 2018. Prevailing winds (~4 ms⁻¹) were from the east and northeast with the average diel temperature of 5°C. To evaluate model-simulated oxidation processes, a series of sensitivity simulations are conducted to compare observed and modeled O₃ and other reactive intermediates. In this case, the model is not constrained with O₃ and PANs observations, whereas NO and NO₂ in the model are scaled to match observed total NO_x. Specific model scenarios are further described in the Supporting Information S1.

3. Results and Discussion

3.1. Measurements

The measured levels of SO₂, CO, organic aerosol (OA), particulate nitrate (NO₃), PANs, NO_x, HONO, O₃, and J-NO₂ during the campaign are shown in Figure 2. High levels of anthropogenic pollutants such as SO₂, CO, and NO_x were frequently observed due to transport from urban areas (Dongying and Ji'nan) and oil and gas (O&NG) fields to the west of the site, in addition, high levels of VOCs (e.g., median propane and toluene levels of 4.35 and 1.71 ppbv) were consistently observed through most of the campaign. On 30% of the days the ozone daily 8-hr average (MDA 8) exceeded 160 μg m⁻³ (~75 ppbv, the Grade II national air quality standard of China) along with enhanced levels of secondary photochemical pollutants such as PAN and its homologs and particulate nitrate (CNEMC, 2018). In addition, biomass burning events were occasionally observed throughout the campaign, consistent with previous work at the same site (Zhang, Sun, et al., 2019).

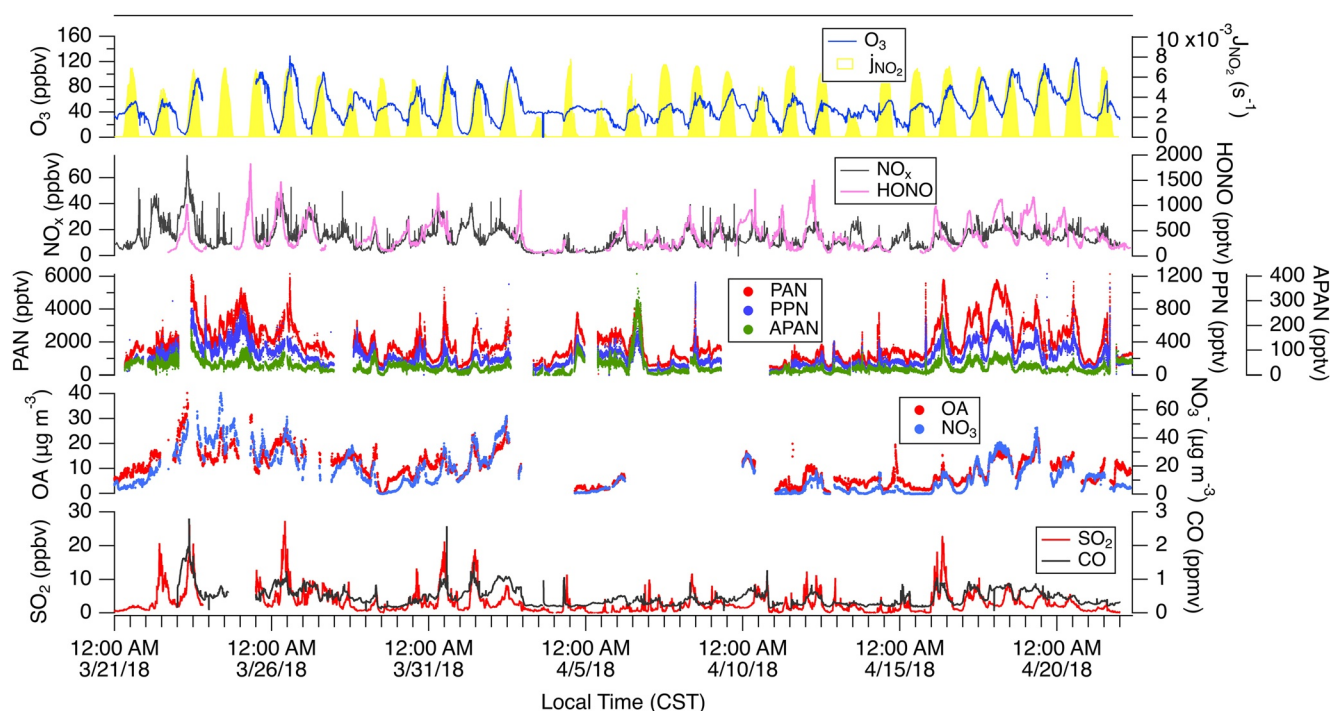


Figure 2. Time series of SO_2 , CO , organic aerosol (OA), particulate nitrate (NO_3^-), PANs, NO_x , HONO, O_3 , and j_{NO_2} measured during OPECE.

3.2. VOCs

Average daytime (10:00–18:00 CST) and nighttime (22:00–6:00 CST) mixing ratios of the measured hydrocarbons are presented in Figure S2a in Supporting Information S1. The highest mixing ratios were observed for the C_2 – C_5 alkanes and C_6 – C_8 aromatics. Mixing ratios of C_2 – C_5 alkanes were highly correlated ($r^2 > 0.8$) with propane throughout the campaign, suggesting they shared a similar source. Mixing ratios of aromatics were better correlated with benzene than propane (Figure S2b in Supporting Information S1). Table 2 summarizes the mixing ratios of VOCs and their correlations with propane and benzene along with rate coefficients for the reactions between VOCs and OH. The magnitude of the alkane mixing ratios and their strong correlation with propane is comparable to observations in oil and natural gas (O&NG) producing areas in the U.S. For example, previous field studies in a O&NG basin in Colorado characterized light alkanes as primary VOC emissions from oil and natural gas operations, with a mean mixing ratio of propane (27 ± 1 ppbv) much larger than observed in U.S. cities (Gilman et al., 2013). Of the measured VOCs, propane and n-butane were the two most abundant with campaign median mixing ratio of 4.3 and 2.6 ppbv, respectively. However, the ratios of both propane and butane to ethane at the site were higher than that in O&NG producing regions in the U.S. (Abeleira et al., 2017; Gilman et al., 2013; Pètron et al., 2012).

Alkenes and aromatics observed at the OPECE site were generally higher than in U.S. O&NG regions. The most abundant alkenes during OPECE were propene and ethene with the campaign median of 0.4 and 0.2 ppbv, respectively. Mixing ratios of isoprene (the campaign median of 0.04 ppbv) were low throughout, suggesting relatively low contributions from biogenic emissions (Zhang, Zhang, et al., 2020). The most abundant aromatics were toluene (the campaign median of 1.7 ppbv) and benzene (the campaign median of 1.2 ppbv) with an average diel maximum of 4.5 and 2.1 ppbv, respectively, in the morning. The higher levels of alkenes and aromatics indicate the OPECE site was likely impacted by urban and industrial (e.g., oil wells and petrochemical facilities) emissions as well.

Mean mixing ratios of selected VOC species observed during the OPECE campaign were compared to the values reported in two polluted urban cities (Houston, Texas, USA and Beijing, China), 28 cities in the U.S., an O&NG producing region in Colorado, and two rural sites (previous measurements at the OPECE site and Changdao) in Shandong province in China (Swarthout et al., 2013) (Figure S3 in Supporting Information S1). As emissions

Table 2
Summary Statistics of Volatile Organic Compound (VOC) Mixing Ratios and Reaction Rate Coefficients With OH

Compound	Mixing ratio (ppbv)		r^2		k_{OH} @ 298K (cm ³ molecule ⁻¹ s ⁻¹)
	Mean (σ)	Median	Propane	Benzene	
Ethane	1 (0.91)	0.76	0.696	0.229	2.48×10^{-13}
Propane	5.61 (4.46)	4.35	1	0.506	1.09×10^{-12}
n-Butane	3.72 (3.53)	2.65	0.932	0.532	2.36×10^{-12}
i-Butane	2.07 (2.11)	1.37	0.913	0.552	2.12×10^{-12}
n-Pentane	1.79 (1.7)	1.25	0.906	0.572	3.8×10^{-12}
i-Pentane	2.3 (2.05)	1.81	0.843	0.538	3.6×10^{-12}
Hexane	0.87 (0.86)	0.65	0.657	0.752	5.2×10^{-12}
2-Methylpentane	0.57 (0.59)	0.4	0.87	0.642	5.2×10^{-12}
3-Methylpentane	0.31 (0.33)	0.22	0.871	0.578	5.2×10^{-12}
2,2-Dimethylbutane	0.066 (0.056)	0.049	0.569	0.564	2.23×10^{-12}
2,3-Dimethylbutane	0.16 (0.15)	0.12	0.788	0.534	5.78×10^{-12}
Heptane	0.21 (0.24)	0.13	0.826	0.514	6.76×10^{-12}
2-Methylhexane	0.071 (0.069)	0.055	0.727	0.682	6.72×10^{-12a}
3-Methylhexane	0.075 (0.095)	0.038	0.567	0.638	6.54×10^{-12a}
2,3-Dimethylpentane	0.043 (0.055)	0.029	0.63	0.382	6.47×10^{-12b}
2,4-Dimethylpentane	0.022 (0.036)	0.012	0.428	0.179	5.64×10^{-12b}
n-Octane	0.21 (0.21)	0.14	0.815	0.535	8.11×10^{-12}
2-Methylheptane	0.046 (0.049)	0.033	0.765	0.529	-
3-Methylheptane	0.028 (0.032)	0.021	0.561	0.436	-
2,2,4-Trimethylpentane	0.1 (0.11)	0.071	0.724	0.501	3.34×10^{-12}
2,3,4-Trimethylpentane	0.03 (0.031)	0.024	0.427	0.41	6.6×10^{-12}
Nonane	0.22 (0.22)	0.15	0.616	0.645	9.7×10^{-12}
Decane	0.27 (0.25)	0.18	0.467	0.6	1.1×10^{-11}
Undecane	0.2 (0.2)	0.14	0.47	0.702	1.23×10^{-11}
Cyclopentane	0.18 (0.21)	0.12	0.852	0.472	4.97×10^{-12}
Methylcyclopentane	0.57 (0.59)	0.39	0.583	0.697	7.65×10^{-12a}
Cyclohexane	0.15 (0.21)	0.089	0.652	0.316	6.97×10^{-12}
Methylcyclohexane	0.14 (0.17)	0.083	0.792	0.299	9.64×10^{-12a}
Ethene	0.27 (0.26)	0.2	0.471	0.727	8.52×10^{-12}
Propene	1.19 (2.44)	0.41	0.363	0.382	2.63×10^{-11}
1-Butene	0.18 (0.3)	0.071	0.467	0.445	3.14×10^{-11}
cis-2-Butene	0.043 (0.11)	0.016	0.355	0.337	5.64×10^{-11}
trans-2-Butene	0.043 (0.11)	0.016	0.354	0.339	6.4×10^{-11}
Pentene	0.065 (0.089)	0.035	0.552	0.573	3.14×10^{-11}
cis-2-Pentene	0.018 (0.028)	0.011	0.473	0.466	6.5×10^{-11}
trans-2-Pentene	0.025 (0.046)	0.014	0.446	0.429	6.7×10^{-11}
Isoprene	0.068 (0.082)	0.04	0.32	0.362	1×10^{-10}
Hexene	0.029 (0.049)	0.02	0.137	0.183	3.7×10^{-11}
Benzene	1.52 (1.09)	1.26	0.506	1	1.22×10^{-12}
Toluene	2.58 (2.69)	1.71	0.441	0.725	5.63×10^{-12}
Ethylbenzene	0.86 (0.81)	0.61	0.295	0.508	7×10^{-12}

Table 2
Continued

Compound	Mixing ratio (ppbv)		r^2		k_{OH} @ 298K (cm ³ molecule ⁻¹ s ⁻¹)
	Mean (σ)	Median	Propane	Benzene	
(<i>m</i> + <i>p</i>)-Xylenes	1.51 (1.57)	0.96	0.274	0.401	1.87×10^{-11}
o-Xylene	0.7 (0.72)	0.72	0.466	0.308	1.36×10^{-11}
Styrene	0.46 (0.51)	0.36	0.32	0.364	5.8×10^{-11}
(<i>m</i> + <i>p</i>)-Diethylbenzene	0.96 (0.66)	0.81	0.315	0.634	-
n-Propylbenzene	0.23 (0.17)	0.2	0.373	0.611	5.8×10^{-12}
i-Propylbenzene	0.038 (0.047)	0.026	0.278	0.403	6.3×10^{-12}
1,2,3-Trimethylbenzene	0.15 (0.2)	0.093	0.436	0.5	3.27×10^{-11}
1,2,4-Trimethylbenzene	0.54 (0.73)	0.33	0.444	0.544	3.25×10^{-11}
1,3,5-Trimethylbenzene	0.18 (0.25)	0.095	0.45	0.543	5.67×10^{-11}
o-Ethyltoluene	0.11 (0.15)	0.059	0.455	0.563	1.19×10^{-11}
(<i>m</i> + <i>p</i>)-Ethyltoluene	0.55 (0.64)	0.36	0.475	0.617	1.52×10^{-11}

Note. Reaction rate coefficients with OH are taken from Atkinson and Arey (2003) unless noted otherwise.

^aSprengnether et al. (2009), ^bWilson et al. (2006).

from oil and gas wells can vary seasonally (e.g., enhanced evaporative emissions from increasing temperature), springtime field data was used for the comparison of O&NG emissions (Abeleira et al., 2017). The alkane mixing ratios were similar to those observed in Houston, Beijing, and Colorado, but generally higher than the average of 28 different U.S. cities (Baker et al., 2008). Highly variable mixing ratios of alkanes have been reported in Shandong province. Recently, Chen et al. (2020) reported a factor of 5–13 higher mean mixing ratios for the selected alkanes at the same site as the OPECE campaign from February to March 2017 than the values observed in this work. On the other hand, the alkane mixing ratios observed at Changdao by Yuan et al. (2013) from March to April 2011 were generally lower than the values in this work. The mean propene and ethene mixing ratios also vary largely between different studies. The propene level during OPECE was similar to the value reported by Chen et al. (2020), 4 to 40 times higher than the level observed in Colorado, and roughly a factor of 2 lower than those observed in Beijing (Li et al., 2015) and Houston (Gilman et al., 2009). The elevated levels of alkenes in Houston have been attributed to petrochemical emissions, whereas emissions from vehicle tailpipe are major sources of alkenes in Beijing (Ryerson et al., 2003; Wang et al., 2015). The mean mixing ratio of toluene and benzene at the OPECE site were more comparable to the mean levels reported for Beijing, Changdao and previous measurements in the YRD by Chen et al. (2020) than the lower levels of toluene and benzene found in most of U.S. cities.

3.2.1. VOC Source Signatures

In previous work, the ratios of ethane to propane and iso-pentane to *n*-pentane have been utilized to investigate the influence of urban and O&NG emissions on ambient air composition (Gilman et al., 2013; Peischl et al., 2013; Swarthout et al., 2013; Wennberg et al., 2012). Though the magnitude of hydrocarbon mixing ratios decreases downwind from source regions, the ratio of VOC pairs that have similar reaction rates with OH (k_{OH}) is minimally affected by air mass mixing, dispersion and photochemical oxidation, and can be used as an indicator of different emission sources (Parrish et al., 2007). Urban areas dominated by vehicle emissions are more enhanced in iso-pentane and ethane, leading to relatively high iso-pentane/*n*-pentane and low propane/ethane ratios (Thompson et al., 2014).

Figure 3 demonstrates these relationships for OPECE by performing orthogonal distance regression (ODR) using the data of VOC pairs measured by GC during the OPECE campaign (Wu & Yu, 2018). The regression slope of propane versus ethane, and iso-pentane versus *n*-pentane were shown along with values reported in a variety of source regions in the U.S. Figure 3a shows that the average propane/ethane ratio is 5.8. This is markedly higher than the values found in Los Angeles, which is primarily impacted by emission from mobile

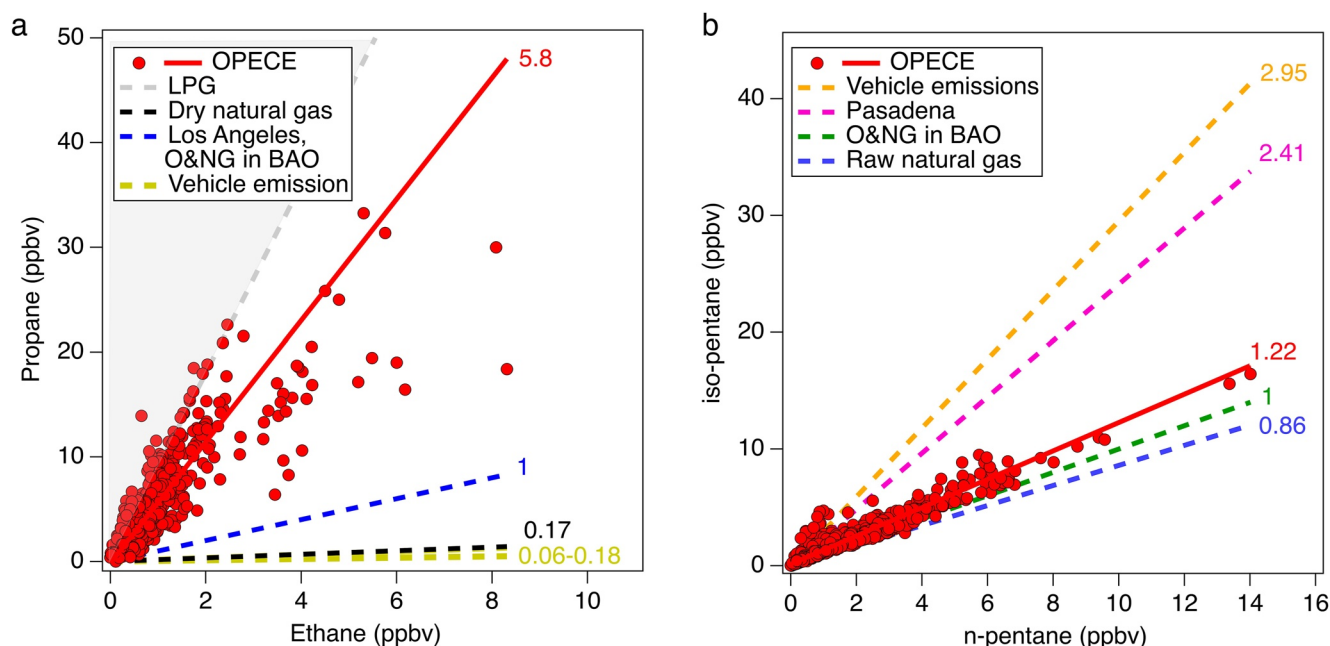


Figure 3. (a) Correlation plots of propane versus ethane for ozone photochemistry and export from China experiment (OPECE) measurement site (red markers and solid red line) and a variety of emission sources. Gray, black, blue, and yellow dashed lines correspond to reported propane-to-ethane ratios from liquified petroleum gas (LPG), dry natural gas, Los Angeles, Boulder Atmospheric Observatory (BAO), and vehicle emissions. (b) Correlation plots of iso-pentane versus n-pentane for OPECE site (red markers and solid red line) compared with values found in the U.S. source regions. Orange, magenta, green and blue dashed lines correspond to reported pentane isomer ratios from vehicle emissions, Pasadena, BAO and raw natural gas emissions. The solid red lines in (a) and (b) are the slope for all campaign data from orthogonal distance regression.

sources and the LPG industry, and in O&NG basins in Colorado (Gilman et al., 2013; Peischl et al., 2013; Pètron et al., 2012; Swarthout et al., 2013; Wennberg et al., 2012). In fact, the OPECE propane/ethane ratio is comparable to the average composition ratio of LPG, which is dominated by propane and butane (Lai et al., 2009; Tsai et al., 2006). For example, Tsai et al., (2006) reported that LPG sold in Hong Kong is mainly propane, butane and iso-butane (>90%), whereas the propane to ethane ratio from dry natural gas after removal of heavy alkanes is ~ 0.17 (Wennberg et al., 2012). Long-term measurements in Hong Kong showed that the contribution of LPG emissions to ambient VOCs increased significantly after the execution of a LPG replacement program for public transportation from 1997 (Ho et al., 2009; Lyu et al., 2016; Ou et al., 2015). The impact of LPG emissions was also indicated by larger abundances of propane and butane isomers than ethane and toluene in Hong Kong (Huang et al., 2015; Ou et al., 2015). Despite the potentially large emissions from LPG sources, the evaluations of the emission inventories in Beijing have demonstrated that natural gas and LPG emissions are largely underestimated (Li, Hao, et al., 2019; Wang, Shao, et al., 2014). On the other hand, vehicular emissions from a tunnel study in the U.S. reported propane/ethane ranging from 0.06 to 0.18 (Lough et al., 2005). Thus, the elevated mean ratio of propane/ethane during the OPECE campaign is significantly different compared to typical urban values, and suggests potentially large contributions of LPG emissions from production (e.g., natural gas processing and petroleum refining), fugitive emissions (e.g., leaks from pipelines, valves, and storage tanks), and fuel consumption (e.g., LPG fueled-vehicle, residential, and industrial usage).

The OPECE *i*-pentane/*n*-pentane ratio was observed to be 1.22 (Figure 3b), which is slightly higher than that in raw natural gas (0.86) and comparable to observations in the northern front range (NFR) in Colorado (1.1–1.17) (Abeleira et al., 2017; Gilman et al., 2013; Swarthout et al., 2013). In urban areas such as Pasadena and Beijing, the pentane isomer ratios range from 1.3 to 4, comparable to the value from vehicle tailpipe emissions of ~ 3 (Barletta et al., 2005; Gilman et al., 2013; Liu, Ma, et al., 2017; Li, Hao, et al., 2019; Thompson et al., 2014). The pentane isomer ratio suggests that the relative contribution of O&NG and mobile sources to pentane was more weighted toward O&NG than for other urban cities in the U.S and China.

3.2.2. Photochemical Removal of VOCs

VOC mixing ratios are impacted by multiple processes such as oxidation, dilution, and emission. The relative importance of the daytime chemical and physical removal of VOCs has been investigated using the diurnal average of VOCs with different chemical reactivity toward hydroxyl radical (OH) (e.g., Borbon et al., 2013; de Gouw et al., 2017). Average diurnal variations of selected VOCs are shown in Figure S4a in Supporting Information S1. The data are averaged in 1-hr bins and normalized to the peak value of each species. The typical diurnal profiles of VOCs at the OPECE site have maximum concentrations during the morning and reduced concentrations in the late afternoon, which can be explained by photochemical removal in combination with dilution in a deeper boundary layer during the day. The more reactive VOCs such as propene and 1, 2, 4-trimethylbenzene had a stronger dependence on the time of day than CO and less reactive VOCs including benzene and propane. Figure S4b in Supporting Information S1 shows the diurnal normalized profiles of selected hydrocarbons relative to CO. The observed mixing ratios of the VOCs to that of CO were more variable for the reactive VOCs, suggesting that photochemical removal affect the observed mixing ratios of these VOCs at the OPECE site.

To further investigate photochemical processing in sampled air masses, the concentration ratios between hydrocarbon pairs with significant differences in OH reaction rate constants were utilized to derive a proxy for photochemical age, hereafter, “OH exposure,” defined as the product of OH concentration and time averaged over the photochemical lifetime of an air mass. OH exposure ($[\text{OH}]\Delta t$) was calculated from the ratio of benzene over 1, 2, 4-trimethylbenzene (124TMB) (Equation 1).

$$[\text{OH}]\Delta t = \frac{1}{k_{124\text{TMB}+\text{OH}} - k_{\text{Benzene}+\text{OH}}} \times \left(\ln\left(\frac{\text{Benzene}}{124\text{TMB}}\right) - \ln(\text{ER}_{\text{Benzene}/124\text{TMB}}) \right) \quad (1)$$

OH reaction rate constants for benzene and 124TMB are from Table 2. The emission ratio ($\text{ER}_{\text{Benzene}/124\text{TMB}}$) is estimated here to be 1.17 ppbv ppbv⁻¹ derived from the slope of scatter plots using the night-time data. Further details are described in Figure S5 in Supporting Information S1. The estimated emission ratio was close to the lower end of the reported range in the U.S, which is from 1.4 to 3.4 ppbv ppbv⁻¹ (Gentner et al., 2013; May et al., 2014; Warneke et al., 2007; Yuan et al., 2012). The average daytime maximum in OH exposure was $\sim 5.5 \times 10^{10}$ molecules cm⁻³ s. The usage of OH exposure derived from hydrocarbon ratios has limitations noted by several studies (de Gouw et al., 2005; McKeen & Liu, 1993; Parrish et al., 2007), largely because the determination of OH exposure does not account for the effects of mixing and transport (i.e., mixing with background air). Thus, OH exposure in this study provides a proxy of photochemical processing for selected VOCs rather than quantitative representation of air mass ages.

Figure 4a gives a scatter plot of hydrocarbons with varying OH rate coefficients color-coded by the OH exposure, where good correlation between two hydrocarbons with similar OH rate coefficients are expected when their removal is largely by reactions with OH. The pentane isomers with similar k_{OH} ($\sim 3.6 \times 10^{-12}$ cm³ molecule⁻¹ s⁻¹) were relatively well correlated ($r^2 = 0.92$). On the other hand, the points in Figure 4b were more widely distributed, and showed a lower *m*, *p*-xylene/benzene ratio at higher OH exposure, which can be explained by a large difference in their k_{OH} (i.e., $k_{\text{m,p-xylene}+\text{OH}} / k_{\text{benzene}+\text{OH}} \sim 15$).

3.2.3. OH Reactivity

OH reactivity is used to investigate ozone production from oxidation of individual hydrocarbons. However, ozone production is a function of various factors including OH levels, ozone yield, and nitrate branching ratios as well as OH reactivity (e.g., Perring et al., 2013).

The total OH reactivity is the summation of individual reactivities calculated by multiplying its concentration ($[X_i]$ in molecules cm⁻³) with the OH rate coefficient ($k_{\text{OH}+X_i}$ in cm³ molecule⁻¹ s⁻¹) provided in Table 2.

$$\text{OH reactivity} = \sum k_{\text{OH}+X_i} \times [X_i] \quad (2)$$

Figure 5 shows the OH reactivity observed during the OPECE campaign along with NO_x and O₃ mixing ratios. The diurnal average OH reactivity including contributions from NO_x and CO was 15.6 ± 4.9 s⁻¹ with a daily

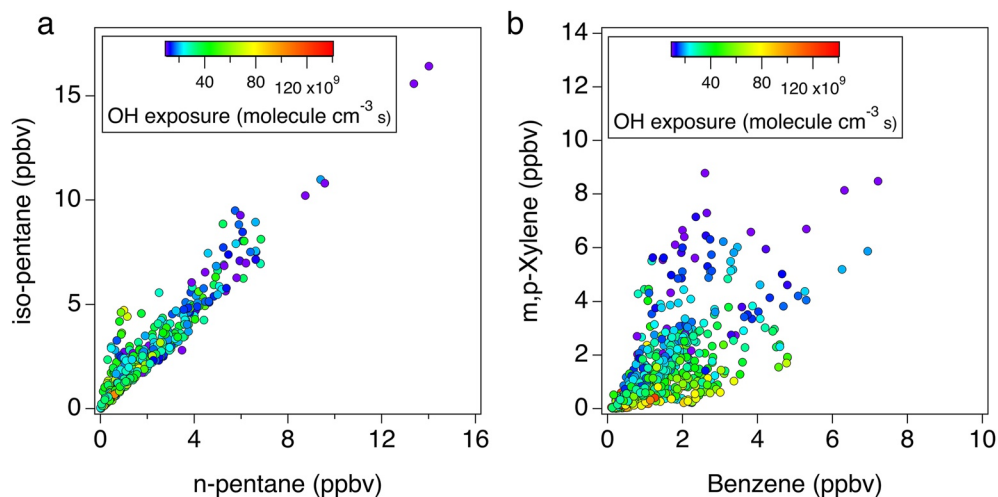


Figure 4. (a) Scatter plot of a hydrocarbon pair with similar (iso-pentane and n-pentane), and (b) different (*m, p*-Xylene and benzene) OH rate coefficients with the data points color-coded by the OH exposure.

maximum average of 23 s^{-1} , where the average contributions from VOCs were $9.1 \pm 3.7 \text{ s}^{-1}$. Aromatics (38%) made the largest contribution to the OH reactivity of VOCs followed by oxygenates (23%), alkanes (20%), and alkenes (19%).

The OH reactivity of VOCs observed at the OPECE site was compared to results from O&NG emission studies in the NFR and Uintah basin (Abeleira et al., 2017; Edwards et al., 2013; Gilman et al., 2013; McDuffie et al., 2016), ground-based measurement at the same study site in the YRD (Chen et al., 2020), recent airborne measurements over Seoul, Korea (Simpson, 2020), and urban/petrochemical studies in Houston (Gilman et al., 2009; Ryerson et al., 2003). In general, the observed OH reactivity at the OPECE site was significantly higher than the reported range ($2\text{--}4 \text{ s}^{-1}$) from O&NG regions in the U.S. A notable difference in the OH reactivity between O&NG regions in the U.S. and OPECE site is a much larger contributions

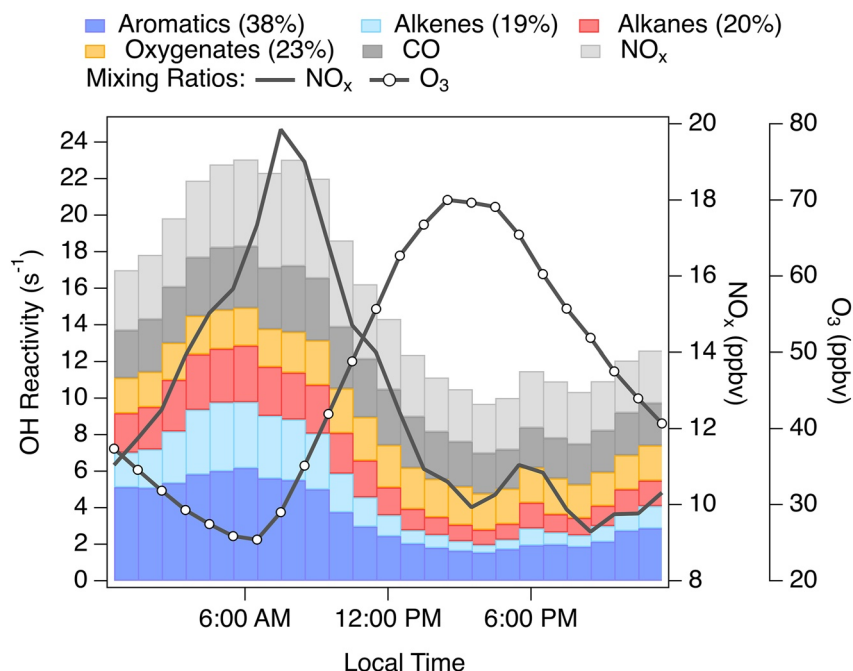


Figure 5. Average diurnal variations (left axis) of calculated OH reactivity including contributions from alkanes, alkenes, aromatics, oxygenates, NO_x and CO. Average diurnal variations of NO_x and O_3 mixing ratios (right axes).

of alkenes and aromatics, especially propene and toluene, at the OPECE site. In the U.S O&NG regions, the dominance of alkanes (>50%) in OH reactivity has been typically observed, where the sum of alkenes and aromatics contribution accounts for ~10% of the OH reactivity reported by McDuffie et al. (2016) and Edwards et al. (2013). In contrast, alkenes and aromatics contribute significantly to OH reactivity in urban areas, where emissions of these compounds are associated with mobile vehicle and industrial sources such as petrochemical facilities (e.g., Borbon et al., 2013; Gilman et al., 2009). Significant enhancements of aromatics and their dominant contributions to OH reactivity are often characteristic of polluted urban emissions in the East Asia. For example, recent airborne measurements during the KORUS-AQ (Korea-United States Air Quality) campaign showed that aromatics and alkenes accounted for 44% and 19% of the average OH reactivity, respectively, over Seoul. These results were consistent with the dominance of aromatics and alkenes on the ozone formation potential in the polluted urban cities on the NCP, China (Li, Hao, et al., 2019; Simpson, 2020; Wu & Xie, 2017). The impacts of more complicated source emissions from mobile vehicles, O&NG production, and petrochemical facilities to air quality have been observed in Houston, TX. The ship-based measurements by Gilman et al. (2009) reported that alkenes and alkanes had a large contribution (41% and 23%, respectively) to the averaged OH reactivity of 7.5 s^{-1} and were due to emissions from mobile vehicles, O&NG productions, and petrochemical refineries. Similarly, airborne plume measurements over Houston Ship Channel shows that alkenes, especially ethene and propene, dominate the OH reactivity ($>15 \text{ s}^{-1}$) in petrochemical plumes, contributing more than 80% (Ryerson et al., 2003).

Similar to the urban areas discussed above, alkenes and aromatics represent a significant fraction of the observed OH reactivity at the OPECE site. The markedly high OH reactivity with elevated NO_x levels during the OPECE campaign was more representative of heavily polluted urban air with complicated source characteristics such as Seoul and Houston than typical U.S. O&NG regions. Chen et al. (2020) pointed out that the OH reactivity at the OPECE site based on their calculations is significantly higher than values reported in rural areas and is comparable to polluted environments such as Beijing and Guangzhou. The OH reactivity by Chen et al. (2020) was comparable to that in this work. However, larger contributions of oxygenated VOCs (OVOC) (including both the observed and model-simulated OVOCs in their calculation) and smaller contributions of aromatics were found in Chen et al. (2020). The observed aromatic contribution to OH reactivity in this work was comparable to those observed in polluted East Asian cities such as Seoul and Beijing than that reported by Chen et al. (2020) (Li, Hao, et al., 2019; Simpson, 2020). While the alkene contribution was also comparable to the urban values, both the remote location of OPECE site with limited mobile vehicle sources and high reactivity of alkenes with OH radicals suggest the impacts of local sources such as petrochemical facilities, (Zhang, Sun, et al., 2019; Chen et al., 2020). The observed OH reactivity at the OPECE site illustrates complicated source emissions from mobile vehicle sources, O&NG production and petrochemical refineries, which are important to understand the photochemistry of this region.

3.3. PANs

PAN and its homologs (i.e., PPN, APAN, PBN, and PBzN) were measured during OPECE. A summary of PANs (PAN + PAN homologs) measured along with their mean and median mixing ratios is presented in Table S2 in Supporting Information S1. PAN was the most abundant peroxyacyl nitrate species measured and comprised ~86% of the total measured PANs. PPN was the most abundant (~80%) of the PAN homologs. Relatively higher mixing ratios of PAN and PPN were observed when the wind was from the west and northwest, whereas the mixing ratios of APAN were more elevated with easterly winds (Figure S6 in Supporting Information S1). Mixing ratios of PANs were generally higher during the day with a diurnal maximum around noon, suggesting photochemical formation following night-time deposition loss in the shallow boundary layer (Figure S7 in Supporting Information S1). There were also periods when PANs mixing ratios did not depend on the time of day and sometimes showed higher median values at night (April 16–April 19, 2018). For these periods, nighttime levels of PANs were relatively well correlated with CO ($r^2 \sim 0.6$), indicating the effects of both photochemistry and transport from upwind sources.

The campaign median PAN and PPN mixing ratios were 1.6 ppbv and 186 pptv, respectively. Both PAN and PPN began to increase in the early morning (6–8 AM) reaching the daytime peak around noon, with a 1-hr averaged

noon-time mixing ratio of 2.2 ppbv and 254 pptv (Figures S7a and S7b in Supporting Information S1). These mixing ratios of PAN and PPN are comparable with polluted urban areas in the U.S. (Los Angeles and Houston in the early 2000s) and East Asia (Beijing and Seoul) (Grosjean et al., 1996; Lee et al., 2008; Qiu et al., 2020; Roberts et al., 2003; Zhang, Zhao, Zhang, 2019). The continual prevalence of elevated PAN and PPN levels at a remote location such as the OPECE site is consistent with a continuous regional influence of urban and O&NG emissions sources.

PBN and APAN were observed up to hundreds of pptv throughout the campaign. PBN and APAN precursors come from a limited range of anthropogenic sources and biomass burning. Mixing ratios of PBN and APAN comparable to the values reported in this study have only been observed in areas strongly impacted by petrochemical emissions and biomass burning emissions (Decker et al., 2019; Roberts et al., 2001, 2003). For OPECE, PBN mixing ratios were measured up to 148 pptv along with large abundances of butane and pentane isomers. This is similar to the reported values during the TexAQs-2000 study, where elevated levels of PiBN observed in Houston were attributed to oxidation of branched-chain alkanes (e.g., isobutane and 2-methyl alkanes) likely from LPG and O&NG emission sources (Roberts et al., 2003). The campaign median APAN mixing ratio (27 pptv) was higher than the values from the ground and airborne measurements (<5 pptv and 8.6 pptv, respectively) in the Houston Ship Channel in 2000. However, episodic increases of APAN levels at the OPECE site resulted in maximum mixing ratios comparable to that in Houston (>400 pptv). These observations are consistent with local sources of APAN precursors such as 1, 3-butadiene and acrolein (Roberts et al., 2001) as the APAN lifetime is relatively short even in cold environments due to its efficient reaction with OH.

The less common PAN homolog, peroxybenzoyl nitrate (PBzN) was monitored as the benzoate ion (m/z 121) in the TD-CIMS. PBzN is the simplest phenyl-substituted peroxyacyl nitrate formed through the oxidation of benzaldehyde, toluene, and styrene. The PBzN signal at m/z 121 was well correlated ($r^2 \sim 0.7$) with PAN. The signal decreased as expected by addition of NO (~ 800 ppm) which reacts with the peroxybenzoyl radical ($C_6H_5C(O)OO$) in the heated inlet (Figure S8 in Supporting Information S1). Zheng et al. (2011) reported the TD-CIMS sensitivity of PBzN was very similar to PAN in a chamber experiment. In addition, Zheng et al. (2011) has also noted possible loss of PBzN on the Teflon inlet wall, which may be partially responsible for no significant levels of PBzN observed in ambient air. Although the inlet losses indicate the potential to underestimate ambient PBzN levels at the OPECE site, the observed levels of PBzN up to ~ 300 pptv may be a representative of markedly different environment in East Asia with enhanced emissions of aromatic precursors of PBzN including toluene and styrene (Fung & Grosjean, 1985). For OPECE, PBzN showed pronounced daytime enhancements with a median of 30 pptv, suggesting local photochemical production of PBzN precursors such as benzaldehyde primarily derived from oxidations of toluene and styrene following the nighttime deposition loss (Figure S7 in Supporting Information S1) (Borbon et al., 2013; de Gouw et al., 2018). Notably, both daytime and nighttime enhancements of PBzN greater than 40 pptv were measured on April 6, 2018 (Figure 6). The nighttime enhancements of PBzN may be indicative of night-time oxidation of precursors that have relatively high O_3 and NO_3 reactivity such as styrene. Currently, field observations of PBzN are quite limited. The only ambient PBzN levels reported in the literature are from Delft, Netherlands (up to 400 pptv) and Los Angeles (0.08–1.81 ppbv) (Fung & Grosjean, 1985; Meijer & Nieboer, 1977).

3.3.1. PANs and O_x

PANs are produced from VOC- NO_x photochemistry, and are closely linked to ozone formation. In general, the daytime (10:00–18:00 CST) average of PANs is well correlated with that of observed odd oxygen ($O_3 + NO_2$; O_x) (Figure 7). However, APAN was found to be only weakly correlated with O_x . This is likely due to a limited range of precursors and the relatively short lifetime of APAN ($\tau_{APAN} < a$ few hours during the day). The positive correlations between PANs and O_x suggest that higher O_3 abundance at the OPECE site is associated with photochemical oxidation of anthropogenic VOCs with the presence of NO_x . For example, PBzN, which can only be formed via aromatic oxidation, was relatively well correlated with O_x , suggesting the effects of photochemical oxidation of reactive aromatics such as toluene and styrene on ozone formation. In addition, Figure 7d shows the relationship of the daytime average ratio of PPN/PAN and PBzN/PAN with that of O_x . Contrary to the negative relationship between PPN/PAN and O_x , PBzN/PAN was positively correlated with O_x . This implies that efficient

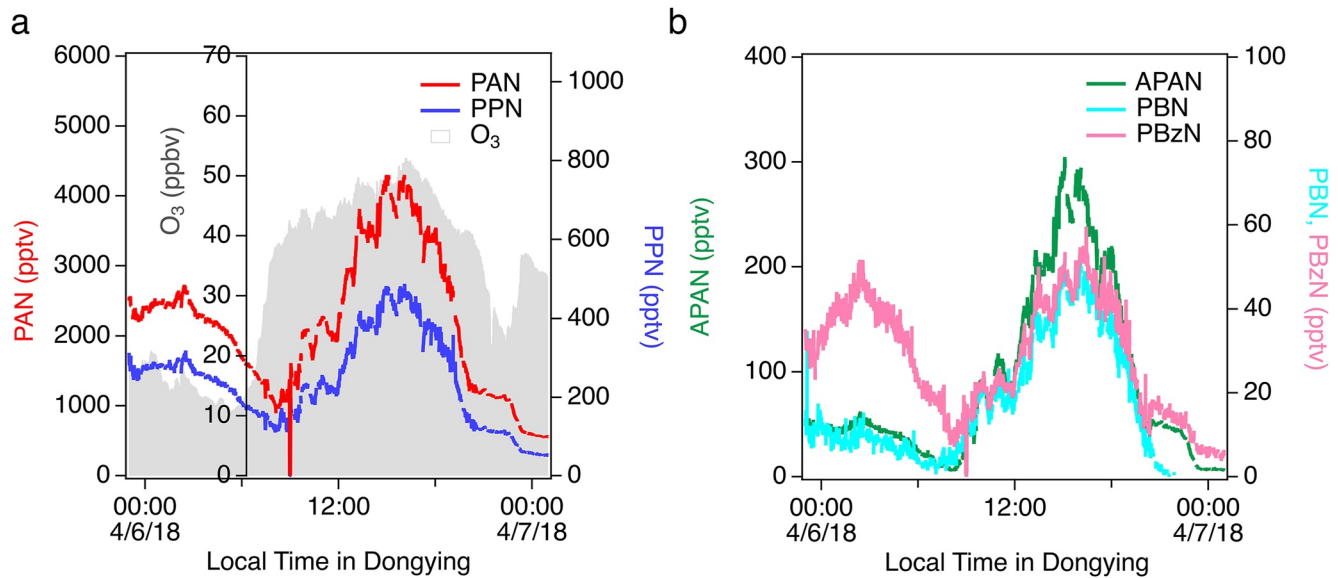


Figure 6. (a and b) Time series of 1-min averaged peroxyacyl nitrates (PANs) (solid lines) and O_3 (gray shaded area) on April 6, 2018. Both PANs and O_3 show daytime enhancements, where peroxybenzoylic nitric anhydride (PBzN) shows both daytime and nighttime enhancements.

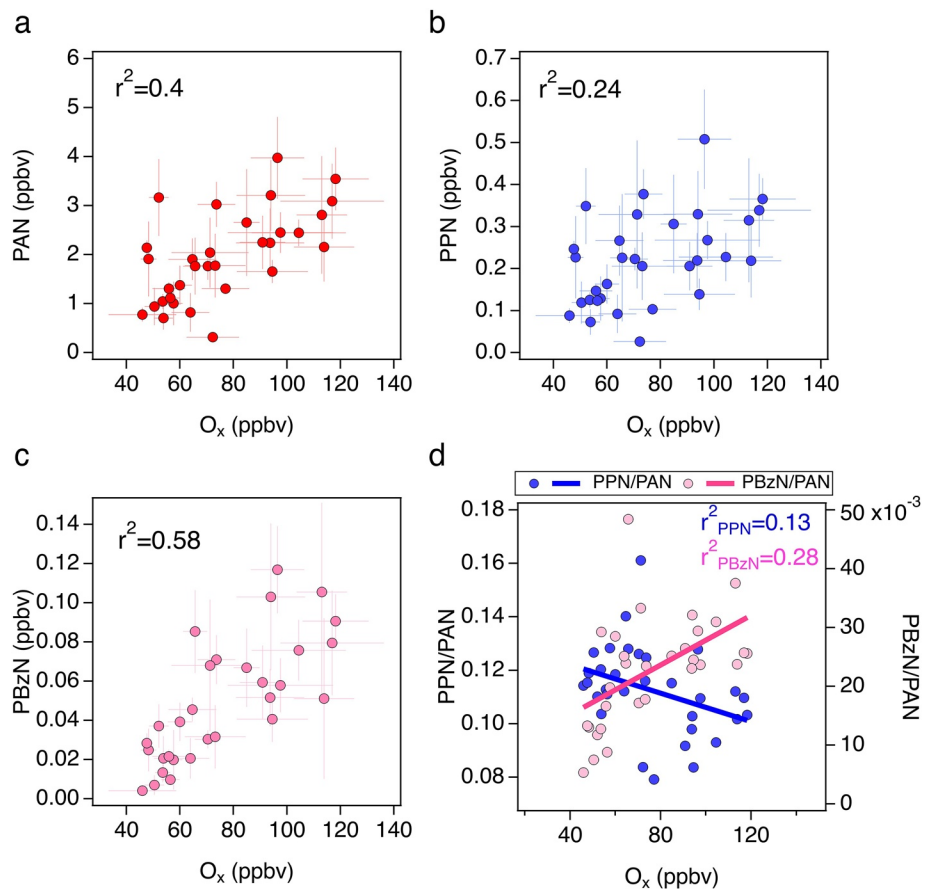


Figure 7. (a–c) Scatter plots of daily daytime (10:00–18:00 CST) average peroxyacyl nitrates (PANs) and O_x mixing ratios with vertical and horizontal lines indicating standard deviations (σ). (d) The ratios of peroxypropionic nitric anhydride (PPN) and peroxybenzoylic nitric anhydride (PBzN) to PAN versus daily daytime average O_x mixing ratios.

radical production from oxidation of aromatics and subsequent radical amplification processes lead to ozone formation while favoring PAN and PBzN formation relative to PPN. Edwards et al. (2013) found that O₃ production in Uintah basin, Utah, was highly sensitive to aromatic concentrations, although the OH reactivity was still dominated by alkanes similar to that in the other US oil production regions. As can be seen from the large fraction of OH reactivity from aromatics (Figure 5) with markedly elevated NO_x levels, radical production from aromatics likely plays an important role in both PAN and O₃ production at OPECE site.

3.3.2. PAN Homologs/PAN

The ratio of individual PAN homologs to PAN potentially provides information on the photo-oxidation of their hydrocarbon precursors. The slope of the scatter plots of PAN versus PAN homologs in Figure 8 were determined using the ODR method and 1-min averaged data of PANs. Figure 8a shows a regression plot of PPN versus PAN. The slope of the regression plot (~12%) falls within the range of typical urban values (10%–15%) in the U.S. (Roberts, 2007) and in East Asian countries (Tanimoto & Akimoto, 2001; Tanimoto et al., 1999; Zhang et al., 2020a). Conversely, the PAN observations during the SOAS 2013 campaign showed that biogenic hydrocarbons accounted for 66% of PAN formation during the campaign with an average PPN/PAN ratio of 4.2%, which is markedly lower than PPN/PAN ratios during OPECE (Toma et al., 2019). While the observed PPN/PAN was similar to the typical urban values in the U.S., a major difference is that the PAN and PPN precursors during OPECE largely originated from urban and O&NG emissions with a large contribution of alkenes and aromatics to OH reactivity. Recently, ground-based PAN measurements in the NFR showed that propane and the larger alkanes from O&NG emissions lead to elevated PPN/PAN ratios (>15%), high ozone events, and OH reactivity dominated by the alkanes (Abeleira et al., 2017; Lindaas et al., 2019; Zaragoza et al., 2017). The observed PPN/PAN ratios during OPECE were relatively lower than that observed in NFR, where the high PPN/PAN ratios indicated photochemistry dominated by the alkanes. This suggests that photochemistry at OPECE is driven by more complicated VOC mixtures including a broad range of alkenes and aromatics that contributes largely to OH reactivity and PAN formation (i.e., Sections 3.2.3 and 3.3.2).

Figure 8b shows a regression plot of PBN versus PAN. On average, PBN showed relatively good correlation with PAN ($r^2 \sim 0.6$) with the slope of the regression plot (~1.5%) comparable to previous measurements (<3%) in the U.S (Roberts et al., 2002, 2003). The observed ratio of PBN/PAN is likely explained by a large abundance of PBN alkane precursors including butane and pentane isomers, and other branched alkanes.

Figure 8c is a regression plot of APAN versus PAN. It should be noted that there are a limited number of data sets of APAN from previous field studies and to our knowledge this study presents first measurement of APAN in China. Most of the time the APAN/PAN ratios during OPECE are between 0.01 and 0.04, similar to previous measurements in a suburban site in Japan and in the Houston Ship Channel in the U.S. (cyan and orange lines in Figure 8c) (Roberts et al., 2001; Tanimoto & Akimoto, 2001). Concurrent measurements of APAN and its hydrocarbon precursors (i.e., 1, 3-butadiene and acrolein) over the Houston Ship Channel showed that background levels (0.019 ppbv) and episodic increases (up to 0.3 ppbv) of APAN were attributed to the impacts from local petrochemical sources of 1, 3-butadiene and acrolein. High levels of APAN were also observed during OPECE with levels up to 400 pptv.

We have also collected an extensive data set of PANs during recent airborne campaigns conducted over Southern California and Seoul, Korea during FIREX-AQ and KORUS-AQ respectively. Figure 8d shows that the slopes of APAN versus PAN are ~1% for both Southern California and Seoul, Korea. For FIREX-AQ, elevated levels of APAN were measured along with enhanced levels of acrolein up to hundreds pptv over Southern California. In addition, the newly reported acrolein emissions ratio ($ER_{\text{acrolein}} \sim 1.4$ pptv ppbv CO) in Pasadena suggests an enhanced importance of 1, 3-butadiene and acrolein in polluted urban atmospheres (de Gouw et al., 2018). However, the study also noted that emissions ratios of aldehydes in Pasadena are much higher than what can be explained from mobile tailpipe emissions, thus their sources in urban air remain unclear (de Gouw et al., 2018; McDonald et al., 2018). For VOCs measurements in China, Yuan et al. (2013) showed average mixing ratios of 1, 3-butadiene (20 ± 20 pptv) and acrolein (90 ± 60 pptv) in Changdao, another rural site located north of OPECE site. These values are high for a remote location considering the high reactivity of these VOCs toward OH (i.e., $k_{1,3\text{-butadiene}+\text{OH}} \sim 6.7 \times 10^{-11} \text{ cm}^3 \text{ molecule}^{-1} \text{ s}^{-1}$; $k_{\text{acrolein}+\text{OH}} \sim 2 \times 10^{-11} \text{ cm}^3 \text{ molecule}^{-1} \text{ s}^{-1}$). During both FIREX-AQ and KORUS-AQ, no significant levels of APAN were measured at remote locations most likely due to its

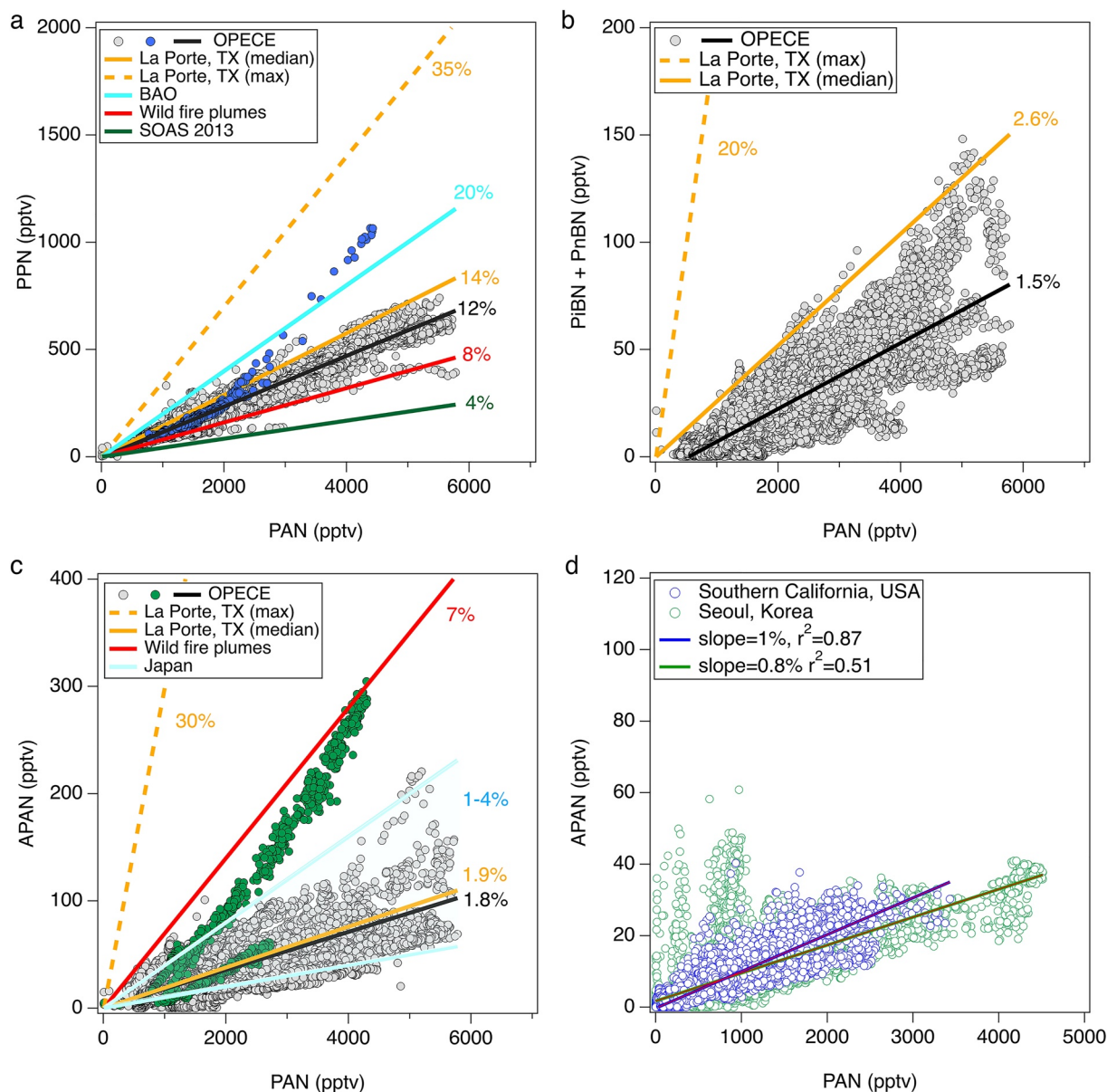


Figure 8. Scatter plots of peroxyacetyl nitrate (PAN) homologs versus PAN. Solid black line indicates PANs/PAN during the ozone photochemistry and export from China experiment (OPECE) campaign (a) Green, red, yellow, and cyan lines correspond to reported peroxypropionic nitric anhydride (PPN)/PAN from Alabama during the SOAS 2013 campaign (Toma et al., 2019), fire plumes during the FIREX-AQ campaign, Houston during the TexAQS 2000 (Roberts et al., 2001) and BAO (Lindaas et al., 2019). (b) Yellow solid and dashed lines correspond to reported median and maximum PiBN/PAN ratio from Houston. (c) Cyan, yellow, and red lines correspond to reported peroxyacrylic nitric anhydride (APAN)/PAN from Japan, Houston, and fire plumes during the FIREX-AQ. The solid blue and green circles in (a) and (c) indicate PPN and APAN data measured during the elevated PPN and APAN episodes on April 8 and April 6, 2018, respectively. (d) Scatter plots of APAN versus PAN measured during the FIREX-AQ (blue circles) and the KORUS-AQ (green circles), which shows airborne data over Southern California and Seoul, respectively.

short lifetime and a lack of precursors. Consequently, the consistent observation of APAN/PAN ratios of $\sim 2\%$ during OPECE suggests the presence of constant sources of 1, 3-butadiene and/or acrolein.

In summary, the large abundance of PANs observed during OPECE were comparable to studies conducted in heavily polluted atmosphere impacted by both urban and industrial emissions including O&NG and petrochemical production. Such high levels of PANs and the correlation of PANs with ozone indicate efficient photochemical oxidation of anthropogenic hydrocarbons from O&NG in the presence of elevated NO_x . The

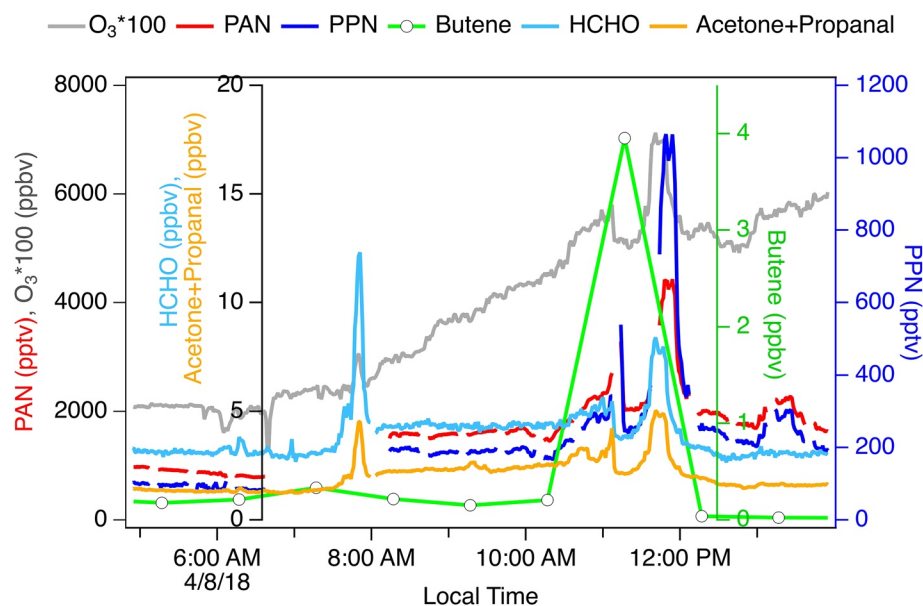


Figure 9. Time series of peroxyacyl nitrate (PAN) (red line), O_3 (gray line), peroxypropionic nitric anhydride (PPN) (blue line), 1-butene (green line with open circle), formaldehyde (cyan line) and acetone + propanal (orange line) on April 8, 2018. Elevated PPN/PAN ratios were observed along with higher mixing ratios of butene isomers (i.e., 1-butene, cis-butene, and trans-butene).

elevated levels of PAN homologs including PBN, APAN, and PBzN are consistent with a complicated VOC profile at the OPECE site.

3.3.3. Elevated PPN/PAN and APAN/PAN Episodes

High PPN/PAN ratios ($\sim 20\%$) (see blue markers in Figure 8a) were measured on April 8, 2018. These high PPN/PAN ratios were associated with easterly and southeasterly winds that were dominated by O&NG emissions (Zhang, Sun, et al., 2019). Figure 9 shows that elevated PPN mixing ratio (1.1 ppbv) observed with excess ozone mixing ratios ($\Delta O_3 = O_{3\text{plume}} - O_{3\text{background}}$) of approximately 18 ppbv. The high PPN/PAN episode were coincident with elevated mixing ratios of butene isomers (i.e., 1-butene, cis-butene, and trans-butene), where the 1-butene mixing ratio (4 ppbv) during the episode was the highest value observed during OPECE campaign. PTR-MS measurement of acetone + propanal and formaldehyde also showed clear enhancements (Figure 9). Within the butene plumes, relatively modest enhancements were observed for CO, SO_2 and NO_x . Biomass burning emissions which can also contain substantial amounts of PANs and ozone, were ruled out because no significant enhancements were measured for acetonitrile (i.e., biomass burning tracer) as well as alkanes and aromatics which can have significant emissions from biomass burning comparable or higher than butene isomers with a relatively longer lifetime (Akagi et al., 2011; Andreae, 2019; Koss et al., 2018). In addition, during the high PPN episodes the ratio of PPN/PAN was significantly higher than typically observed in fire plumes (0.08–0.1) (e.g., Roberts et al., 2004; airborne plume measurements during FIREX-AQ). The significant enhancements of alkenes (i.e., butene), PPN and ozone suggest that air masses were likely impacted by O&NG emission sources such as petrochemical facilities (Roberts et al., 2003; Ryerson et al., 2003; Wert et al., 2003).

Elevated APAN/PAN ratios (0.06) were observed for a continuous period during April 6, 2018 (Figure 6b and green markers in Figure 8c). For this episode, the diurnal variations of PANs and O_3 showed pronounced enhancements in the afternoon, suggesting photochemical formation of these species. The high APAN/PAN ratio suggests photo-oxidation of 1, 3-butadiene and/or acrolein, which are petrochemical emissions (Roberts et al., 2001). No significant elevation was observed for acetonitrile for this day. Contributions of long-range transport of APAN and APAN precursors from upwind urban areas should be small due to fast oxidation by OH radicals ($\tau_{\text{APAN and its precursors}} < \text{a few hours}$). Whereas it is difficult to explain the high APAN/PAN episode without direct measurement of 1,3-butadiene and acrolein, the high APAN/PAN episode suggests possible systematic

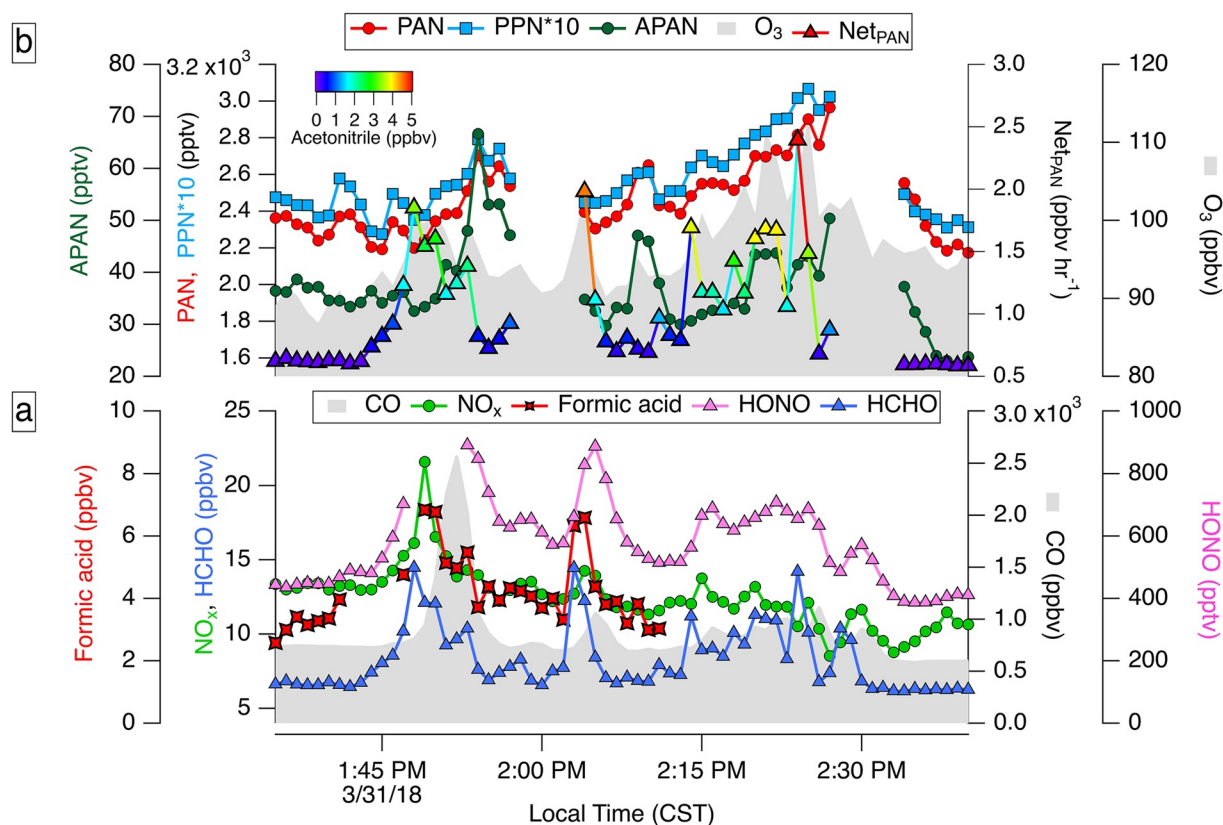


Figure 10. 1-min averaged measurements within biomass burning plumes. (a) Time series show significant enhancements of CO (gray shaded area), NO_x (green circles), HCHO (blue triangles), HONO (pink triangles), and formic acid (red markers) within the plumes of the bird sanctuary fire on March 31, 2018. (b) Timeseries of peroxyacyl nitrate (PAN) (red circles), peroxypropionic nitric anhydride (PPN) multiplied by 10 (light blue squares), peroxyacrylic nitric anhydride (APAN) (green circles), and O₃ (gray shaded area) along with Net PAN production rate (triangles) color coded by the measured mixing ratios of acetonitrile.

increase in APAN carbonyl precursors from local sources and their contributions to VOC-NO_x photochemistry at OPECE site.

3.4. Impacts of Biomass Burning on O₃ and PANs

Biomass burning emits significant amounts of organic compounds and NO_x, which can undergo photo-oxidation and produce O₃ and reactive nitrogen (NO_y) (Alvarado et al., 2010; Andreae, 2019; Crutzen & Andreae, 1990). Throughout the campaign, biomass burning events occurred occasionally around the study region (Figure S9 in Supporting Information S1). For example, a fire in the bird sanctuary near the measurement site started in the early morning on March 31, 2018 and grew in intensity through the day. The fire was located ~3 km south of the measurement facility and burned mainly grass. Pictures of the bird sanctuary fire are shown along with fire hot-spot data from MODIS Fire Information for Resource Management System (FIRMS) in Figure S9 in Supporting Information S1.

Figure 10a shows significant enhancements of CO, NO_x, HCHO, HONO, and formic acid within the plumes of the bird sanctuary fire. These compounds can be emitted directly from fires and formed by photochemistry (i.e., HCHO, HONO, and formic acid) (Akagi et al., 2013; Liu et al., 2016; Liu, Huey, et al., 2017; Yokelson et al., 2009).

A large fraction of initial NO_x emissions from fires can be converted to other NO_y species including HNO₃, PANs and particulate nitrate (Alvarado et al., 2010). Figure 10b shows enhancements of PAN, PPN and APAN up to 693, 66, and 36 pptv, respectively, above their background mixing ratios (2273, 241, and 30 pptv, respectively), which were determined based on average of measurements made 10 min before and after the plume encounter.

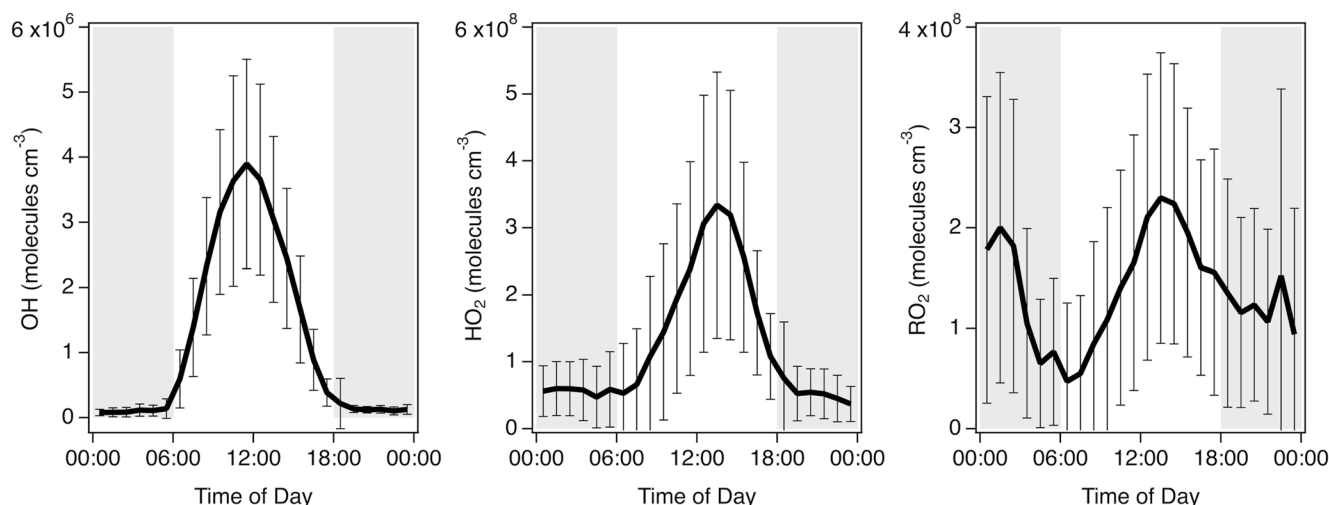


Figure 11. Average diurnal variations of modeled OH, HO₂, and RO₂ concentrations (black lines) in the base case model scenario. The vertical error bars show the hourly standard deviation (σ), and the gray shaded area indicates nighttime.

O₃ production is also common from biomass burning plumes. O₃ was also elevated up to 21 ppbv above its background mixing ratio of 92 ppbv within plumes from the bird sanctuary fire. The instantaneous PAN production rate from the oxidation of acetaldehyde was estimated for the plumes from the bird sanctuary fire. Net_{PAN} (i.e., Net_{PAN} = P_{PAN} - L_{PAN}) was estimated using Equations 3 and 4, where the NO_x, acetaldehyde and PAN concentrations were from 1-min averaged in situ measurements, and an average daytime OH concentration of 2.5×10^6 molecules cm⁻³ was estimated using 0-D box model simulations.

$$\beta = \frac{k_{\text{PA}+\text{NO}_2} [\text{NO}_2]}{(k_{\text{PA}+\text{NO}_2} [\text{NO}_2] + k_{\text{PA}+\text{NO}} [\text{NO}])} \quad (3)$$

$$\text{Net}_{\text{PAN}} = \beta k_{\text{CH}_3\text{CHO}+\text{OH}} [\text{CH}_3\text{CHO}] [\text{OH}] - k_{\text{PAN} \rightarrow \text{PA}+\text{NO}_2} (1 - \beta) [\text{PAN}] \quad (4)$$

Within the plume, Net_{PAN} was well correlated with acetonitrile (triangle markers colored by acetonitrile mixing ratios in Figure 10b). The elevated Net_{PAN} up to 2.4 ppbv hr⁻¹ within the plume was markedly higher than that of campaign daytime average (334 ± 272 pptv hr⁻¹). The elevated Net_{PAN} was due to the enhancements in acetaldehyde and NO₂ to NO ratios in the fire plumes increasing production rates of PAN.

3.5. Diagnostic 0-D Box Model Simulations

3.5.1. Model Simulated Concentration of OH, HO₂, and RO₂

The model calculated average diurnal profiles of OH, HO₂, and RO₂ concentrations for the full campaign period are shown in Figure 11. The model outputs using the 10-min averaged observational constraints of the full campaign are averaged in 1-hr bins to produce the diurnal profiles in Figure 11, and refer to the base case scenario. The average maximum concentrations were 3.9×10^6 molecules cm⁻³ for OH around noon and 3.3×10^8 molecules cm⁻³ and 2.3×10^8 molecules cm⁻³ for HO₂ and RO₂, respectively, in the early afternoon. In general, predicted OH levels were the highest on days with lower VOC levels and high photolysis rates. The modeled HO₂ and RO₂ concentrations did not show a significant difference between clean and polluted episodes. An additional rise in modeled RO₂ concentrations throughout the nighttime was due to oxidations of reactive alkenes and styrene by O₃ and NO₃ (nitrate radical). It should be noted that the fluctuation of NO measurements often below the detection limit (~ 100 pptv) during night-time also resulted in variability in model calculations of NO₃ and RO₂ concentrations (Tan et al., 2017, 2018). In addition, the sensitivity analysis to examine the potential positive interference in NO₂ measurements showed <5% and <12% decrease in radical concentrations (OH, HO₂, and RO₂) with 10% and 20% decrease in the observed NO₂ constraint, respectively.

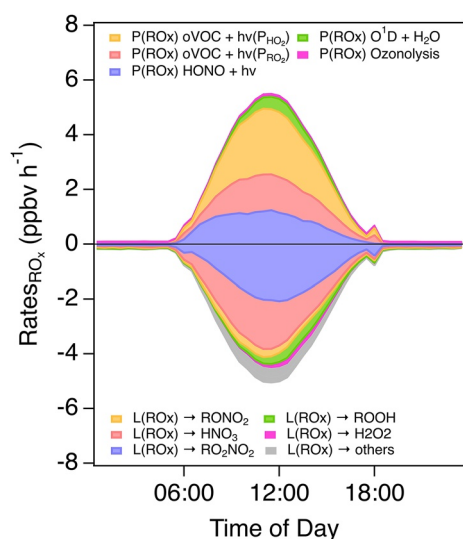


Figure 12. The diurnal average sources and sinks of RO_x (OH + HO₂ + RO₂) versus time of day. The model calculated radical production and loss rates are averaged in 1-hr bins. The color-shaded regions where rates are positive are sources and where they are negative are sinks. No heterogeneous process (e.g., deposition, loss on aerosol) are included in the model calculations.

Compared to other radical measurements conducted over mainland China, the predicted noontime OH, HO₂ and RO₂ concentrations during OPECE were close to the median values measured in the Pearl River Delta in autumn 2014 (Tan, Lu, Hofzumahaus, et al., 2019). The noontime OH concentration observed in Wangdu in summer 2014 (Tan et al., 2020) and in Beijing in winter 2016 (Tan et al., 2018) were 8×10^6 molecules cm⁻³ and 2.8×10^6 molecules cm⁻³, which were approximately a factor of 2 higher and 25% lower than the noontime modeled OH levels during the OPECE campaign, respectively. Radical measurements conducted over oil and gas fields are still sparse. Kim et al. (2014) reported the observed wintertime OH concentrations of $\sim 2.7 \times 10^6$ molecules cm⁻³ at noon in the NFR from NACHTT-11 (Nitrogen, Aerosol Composition, and Halogens on a Tall Tower 2011) campaign, which is 30% lower than the noontime modeled OH levels in this work.

3.5.2. Sources and Sinks of RO_x

Figure 12 shows the diurnal average of primary sources and sinks of RO_x (OH + HO₂ + RO₂) radical derived from the full-campaign model simulations. The model calculated rates of radical production and loss using the full campaign observational constraints are averaged in 1-hr bins. RO_x radical production includes photolysis of OVOCs, HONO and O₃ (followed by O¹D + H₂O), and the reactions of O₃ and nitrate radical with hydrocarbons.

Loss processes for RO_x include formation of radical reservoir species such as nitric acid (HNO₃) and peroxides (H₂O₂ and ROOH). At colder ambient temperatures, the net radical loss also includes NO_x-RO₂ reactions producing peroxy nitrates (RO₂NO₂), mostly consisting of PANs.

Photolysis of OVOCs was the primary source of RO_x contributing 3.7 ppbv hr⁻¹ for the sum of HO₂ (2.4 ppbv hr⁻¹) and RO₂ production (1.3 ppbv hr⁻¹) at noon. Photolysis of HCHO contributed $\sim 50\%$ of HO₂ production rates, followed by that of methyl glyoxal ($\sim 20\%$). HONO photolysis was the second largest source of RO_x (1.2 ppbv hr⁻¹ at noon) and the largest source of OH. Similarly, Chen et al. (2020) pointed out that photolysis of OVOCs and HONO are the dominant radical source during the winter-springtime field campaign at the OPECE site in 2017. In a sensitivity test, not constrained by observed HONO, modeled OH concentrations decreased by 35% compared to those in the base case model scenario, while modeled HO₂ and RO₂ concentrations decrease by 24% and 26%, respectively, in the sensitivity test without the observed HONO constraint (Figure S10 in Supporting Information S1). On average, the average daytime OH production rate from HONO photolysis (0.8 ppbv hr⁻¹; 5.2×10^6 molecules cm⁻³ s⁻¹) during OPECE was higher than the observed average rate in Beijing (0.3 ppbv hr⁻¹) and NFR (3.1×10^6 molecules cm⁻³ s⁻¹) in the wintertime (Kim et al., 2014; Tan et al., 2018). Production of OH from O₃ photolysis (O¹D + H₂O) was also an important source of OH with rate of 0.5 ppbv hr⁻¹ at noon. Minor RO_x sources including ozonolysis and nitrate radical oxidations of alkenes and styrene were more important at night.

The loss of RO_x was dominated by NO_x reactions at the OPECE site. The net formation of RO₂NO₂ (2.4 ppbv hr⁻¹ at noon) was the largest loss of RO_x during OPECE, followed by the reaction of OH with NO₂ producing HNO₃ (1.8 ppbv hr⁻¹ around noon). On average, PAN production contributed $\sim 50\%$ of total RO₂NO₂ production rates, followed by PPN production ($\sim 10\%$). Notably, production of PBzN was comparable to that of PPN, due to elevated benzaldehyde from the oxidation of styrene and toluene. In a sensitivity test without aromatics, the daytime PAN and PPN production decreased by 75% and 45%. The larger decrease in PAN production than PPN was due to a large reduction in methyl glyoxal (93%). Therefore, the model simulation generally suggests that radical sources such as methyl glyoxal derived from the oxidation of aromatics affect the modeled production and distribution of reactive nitrogen. Another loss process of RO_x was by RONO₂ production (average of 0.3 ppbv hr⁻¹ in the morning from 6:00 to 9:00 CST), which was smaller than RO₂NO₂ production. In contrast to the large radical loss by formation of NO_x oxidation products (NO_z), the radical loss by radical-radical reactions producing peroxides (average of 0.6 ppbv hr⁻¹ around noon) was much lower, whereas this radical-radical reactions are the dominant radical termination mechanism in the YRD in summer (Chen et al., 2020). The dominant

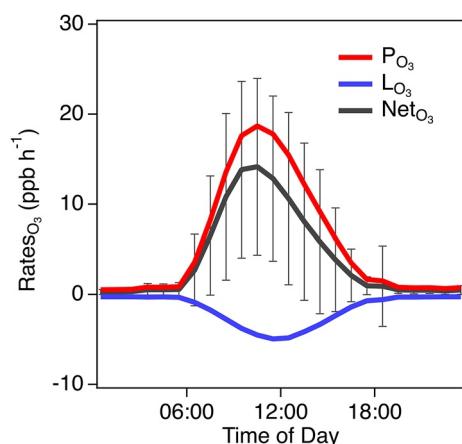


Figure 13. Calculated diurnal variation of average production rates (red line), loss rates (blue line) and net rates (black line) of O_3 . The vertical error bars show the hourly standard deviation (σ) of the means.

loss of radicals via reaction with NO_x during springtime suggests characteristics similar to NO_x -rich urban environments (Tan et al., 2018).

3.5.3. O_3 Formation Rate and Production Efficiency

Boundary layer O_3 concentrations are a complicated function of both chemical and physical process such as chemical production, deposition, advection and vertical mixing. Simulation of the ambient rate of change in O_3 levels requires complicated treatment of these processes often using chemical transport models (CTMs). In this work, we focus on the calculation of the production rate of ozone, $P(O_3)$, which is an important factor governing surface ozone levels. The model results shown hereafter provide a diagnostic analysis to investigate VOC- NO_x photochemistry leading to ozone formation at the OPECE site utilizing the extensive set of observational constraints and a near-explicit chemical mechanism.

Figure 13 shows the full-campaign diurnal average $P(O_3)$. $P(O_3)$ was determined as the rate of reaction of peroxy radicals (HO_2 and RO_2) with NO . The daytime (10:00–18:00 CST) average $P(O_3)$ was 10.6 ppb hr^{-1} with a maximum of 18.7 ppb hr^{-1} that occurred before noon CST. The rates of reaction of HO_2 and RO_2 with NO contributed 54% and 46% of the modeled $P(O_3)$, respectively. The daily maximum modeled $P(O_3)$ and its peak time during OPECE were similar to recent measurements of $P(O_3)$ in Beijing ($\sim 16 \text{ ppb hr}^{-1}$) and NFR ($\sim 14 \text{ ppb hr}^{-1}$) (Tan et al., 2018; Baier et al., 2017). Previous measurements of $P(O_3)$ in Beijing, NFR and other urban studies have noted that the measured $P(O_3)$ was markedly higher than model estimations in the early morning when NO_x levels were high (Baier et al., 2017; Cazorla et al., 2012; Tan et al., 2018). The daytime (10:00–18:00 CST) average $L(O_3)$, loss rate of O_3 , was 3.3 ppb hr^{-1} with a daily maximum of 5 ppb hr^{-1} at around 12:00 CST. $L(O_3)$ is dominated by the reactions of $OH + NO_2$ (46%), $RO_2 + NO_2$ (33%), $O^1D + H_2O$ (6%). The remaining $L(O_3)$ is due to reactions of O_3 with OH , HO_2 , and VOCs (15%). The daytime (10:00–18:00 CST) average net O_3 production, that is, $P(O_3) - L(O_3)$, was 7.3 ppb hr^{-1} with a maximum of 14.2 ppb hr^{-1} .

The comparison of the simulated chemical production rate of ozone with the ambient rate of change is complicated due to physical processes such as dilution, advection, and deposition, which are not explicitly accounted for in the chemical model. Such comparison requires detailed analysis using CTMs. Instead, a diagnostic model case study was performed to investigate the observed and model-simulated photochemistry leading to formation of O_3 and reactive intermediates such as PANs on April 6, 2018, when local photochemistry might be more important relative to other measurement period (Section 2.3 and Supporting Information S1). For the diagnostic model simulations, a first order loss equivalent to a 12-hr lifetime was necessary to reasonably reproduce the observed O_3 , PAN, and PPN (Figure S11 in Supporting Information S1).

In addition to estimation of $P(O_3)$, ozone production efficiency (OPE) was estimated by dividing $P(O_3)$ by the rates of NO_x oxidation to HNO_3 , RO_2NO_2 and $RONO_2$ (i.e., NO_2). The daytime OPEs were in the range of 1.2–9.4 with the daytime average and diel maximum of 3.3 and 4.7, respectively. The daytime average OPEs during OPECE was similar to that of a NO_x -rich polluted urban region (<5) (Kleinman et al., 2002). Namely, the OPEs fall within the reported range for polluted cities in China and U.S., for example, 2.2 in Guangzhou (Tan et al., 2019a), 3–6 in Beijing (Tan et al., 2019a; Wang et al., 2010), 2.2–4.2 in New York (Kleinman et al., 2000), and 2.6–10 for petrochemical plumes in Houston (Daum et al., 2003).

3.5.4. Chemical Regimes of O_3 Production

The photochemistry of O_3 is complex and depends non-linearly on precursor concentrations. To formulate effective mitigation strategies, it is necessary to understand whether local O_3 photochemistry is NO_x -limited or VOC-limited (Sillman et al., 1990). We examine the sensitivity of $P(O_3)$ to perturbations of NO_x and VOCs concentrations. The average relative changes of $P(O_3)$ compared to base case scenario, $\Delta P(O_3)$, were evaluated when model inputs for NO_x and VOCs were varied 120%, 110%, 90%, 80%, and 60% of the base model constraints.

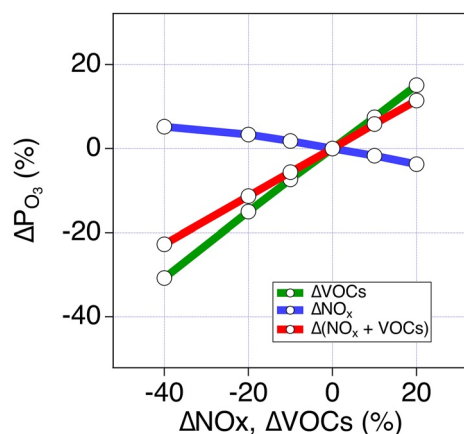


Figure 14. The average relative changes of modeled $P(O_3)$ compared the base case scenario, $\Delta P(O_3)$ as a function of changes of NO_x and volatile organic compounds (VOCs) levels calculated for 60%, 80%, 90%, 110%, and 120% of the base case conditions.

Figure 14 shows $\Delta P(O_3)$ with respect to the change of NO_x and VOCs (i.e., ΔNO_x and $\Delta VOCs$). $P(O_3)$ consistently shows negative response to ΔNO_x . In other words, reductions in NO_x for a given VOC abundance results in an increase in $P(O_3)$. Upon reducing NO_x by 40%, $\Delta P(O_3)$ was higher than the base simulation by 5% on average. This also indicates that our findings of the model-simulated chemical regime for $P(O_3)$ are still valid even for a potential 20% positive interference in NO_2 measurements. The sensitivity of $\Delta P(O_3)$ showed a positive and linear response to $\Delta VOCs$, therefore, indicating a radical-limited (i.e., VOC-limited) environment. This is in accord with the results from the similar modeling analysis by Chen et al. (2020), where the reactions between RO_x and NO_x are the dominant radical sinks for winter-springtime YRD due to elevated levels of NO_x . Concurrent reduction of NO_x and VOCs concentrations were less effective in reducing $P(O_3)$ compared to when only VOCs concentrations were reduced.

4. Summary and Conclusions

This study provides an extensive data set of primary emissions and secondary photochemical products measured in the Yellow River Delta downwind from urban and O&NG emissions during OPECE. We report mixing ratios of over 50 hydrocarbon species, which are compared with those from previous studies in urban and O&NG producing regions in the U.S. and China. Even though the OPECE site is a remote location, the observed VOCs mixing ratios were comparable to those measured in heavily polluted cities such as Houston and Beijing. Consistent with previous VOCs measurements conducted in East Asia, a large abundance of aromatic hydrocarbons was a distinguishing feature at OPECE site. The source signatures of VOCs suggest strong influence from O&NG emissions. The pentane isomer ratios at the OPECE site were in accord with those of U.S. O&NG fields. The markedly high propane-to-ethane ratios along with large abundance of C_4 - C_5 alkanes were likely associated with LPG emissions. In general, the diurnal variations of reactive hydrocarbons showed significant variability due to the photochemical oxidation by OH. The highly elevated levels of VOCs, especially aromatics and alkenes, along with NO_x contributes to significantly higher OH reactivity than that found in the U.S. O&NG regions.

Measurements of PANs allowed a detailed investigation into the VOC- NO_x photochemistry leading to ozone and reactive nitrogen production. The prevalence of elevated PAN and PPN levels at a remote location such as the OPECE site is consistent with a continuous influence of urban and O&NG emissions sources, and their subsequent photochemistry over a large region. The correlation between daytime PANs and O_x indicates the impacts of VOCs- NO_x photochemistry on PANs and ozone production. A strong positive correlation between O_x and PBzN with the increasing and decreasing ratios of PBzN/PAN and PPN/PAN, respectively, as a function of O_x may be indicative of ozone production at OPECE that is sensitive to reactive aromatic emissions such as toluene and styrene. Episodic elevations of PPN and APAN were also observed and are likely associated with petrochemical emissions. Biomass burning events were occasionally observed throughout the campaign period and were indicated by rapid enhancements of ozone and PANs along with acetonitrile, CO, HONO, NO_x and formic acid. Consequently, the detailed analysis of PANs was consistent with many of the features in VOCs measurements in different pollution episodes, suggesting the utility of PANs as a tracer to help understand the complex photochemistry in polluted and heterogeneous VOC environments such as the OPECE site.

Diagnostic model simulations using a near-explicit 0-D chemical box model were performed to investigate the budgets of RO_x ($OH + HO_2 + RO_2$) and production rate and efficiency of O_3 . The model calculated OH, HO_2 and RO_2 peaked around noon were similar to the values measured at the Pearl River Delta in autumn (Tan, Lu, Hofzumahaus, et al., 2019) and ~40% higher than the wintertime OH concentrations in NFR. The RO_x production was dominated by photolysis of OVOCs, HONO, and O_3 , where the reactions of radicals with NO_x producing HNO_3 and RO_2NO_2 were the dominant loss process. The simulated daytime average $P(O_3)$ was 10.6 ppb hr^{-1} with a daily maximum of 18.7 ppb hr^{-1} comparable to the recent measurements of $P(O_3)$ in Beijing ($\sim 16 \text{ ppb hr}^{-1}$) and NFR ($\sim 14 \text{ ppb hr}^{-1}$). The daytime average OPEs during OPECE were similar to that of a NO_x -rich urban region (<5) such as Guangzhou, Beijing, New York and Houston. In addition, we examined the sensitivity of

$P(O_3)$ to perturbations of NO_x and VOCs concentrations. $P(O_3)$ consistently showed a negative response to ΔNO_x , indicating reductions in NO_x will increase $P(O_3)$, and the ozone production at OPECE site is in a VOC-limited or NO_x saturated regime.

In conclusion, the OPECE site is characterized by near continuously elevated levels of VOCs and NO_x due to urban and O&NG emission sources. Similar to other O&NG studies, the shorter-chained alkanes (C_2 - C_4) showed the largest abundance on a molar basis. However, aromatics and alkenes also represent a significant fraction of the reactivity with OH and make a large contribution to ozone production. Consistent elevation of PANs further points to the photooxidation of these aromatics and alkenes. Both VOCs and PANs measurements indicate the strong influence of urban and O&NG emissions which is comparable to studies conducted in heavily polluted atmosphere such as Houston in the early 2000s. Box model simulations constrained by observations suggest that ozone production at OPECE site is VOC-limited in spring, which is similar to the findings from other polluted urban cities and O&NG producing regions such as Seoul, Houston, and Uintah basin (e.g., Edwards et al., 2013; Ryerson et al., 2003; Schroeder et al., 2020) and previous study at the OPECE site (Chen et al., 2020). This suggests that reduction in VOCs emissions, especially C_{7+} aromatics and alkenes, should be a priority for reducing O_3 at the OPECE site. Production (e.g., oil and gas extraction and petrochemical refining) and fugitive emissions (e.g., leakage from pipelines, valves and storage tanks) provide an attractive target for emission reduction. To fully access the effects of emission reductions on air quality of the OPECE site, chemical transport modeling that implements chemistry, emissions and transport is necessary, and the measurements during the OPECE campaign can provide a valuable data set to evaluate future model analyses.

Data Availability Statement

All of the data used in this work are available from: https://glacier.cos.gatech.edu/opece/Data_OPECE.xlsx.

Acknowledgments

The OPECE field campaign was supported by NSF grant 1743401. The authors thank David Parrish for comments on our analyses and manuscript. The authors thank the Yellow River Delta Ecological Research Station of Coastal Wetland, which belongs to the Yantai Institute of Coastal Zone Research, Chinese Academy of Sciences, for logistical support during the campaign.

References

- Abeleira, A., Pollack, I. B., Sive, B., Zhou, Y., Fischer, E. V., & Farmer, D. K. (2017). Source characterization of volatile organic compounds in the Colorado Northern Front Range Metropolitan Area during spring and summer 2015. *Journal of Geophysical Research: Atmospheres*, 122, 3595–3613. <https://doi.org/10.1002/2016JD026227>
- Akagi, S. K., Yokelson, R. J., Burling, I. R., Meinardi, S., Simpson, I., Blake, D. R., et al. (2013). Measurements of reactive trace gases and variable O_3 formation rates in some South Carolina biomass burning plumes. *Atmospheric Chemistry and Physics*, 13(3), 1141–1165. <https://doi.org/10.5194/acp-13-1141-2013>
- Akagi, S. K., Yokelson, R. J., Wiedinmyer, C., Alvarado, M. J., Reid, J. S., Karl, T., et al. (2011). Emission factors for open and domestic biomass burning for use in atmospheric models. *Atmospheric Chemistry and Physics*, 11(9), 4039–4072. <https://doi.org/10.5194/acp-11-4039-2011>
- Alvarado, M. J., Logan, J. A., Mao, J., Apel, E. C., Riemer, D., Blake, D., et al. (2010). Nitrogen oxides and PAN in plumes from boreal fires during ARCTAS-B and their impact on ozone: An integrated analysis of aircraft and satellite observations. *Atmospheric Chemistry and Physics*, 10(20), 9739–9760. <https://doi.org/10.5194/acp-10-9739-2010>
- Andreae, M. O. (2019). Emission of trace gases and aerosols from biomass burning: An updated assessment. *Atmospheric Chemistry and Physics*, 19, 8523–8546. <https://doi.org/10.5194/acp-19-8523-2019>
- Atkinson, R., & Arey, J. (2003). Atmospheric degradation of volatile organic compounds. *Chemical Reviews*, 103(12), 4605–4638. <https://doi.org/10.1021/cr0206420>
- Bahreini, R., Ahmadv, R., McKeen, S. A., Vu, K. T., Dingle, J. H., Apel, E. C., et al. (2018). Sources and characteristics of summertime organic aerosol in the Colorado Front Range: Perspective from measurements and WRF-Chem modeling. *Atmospheric Chemistry and Physics*, 18, 8293–8312. <https://doi.org/10.5194/acp-18-8293-2018>
- Baier, B. C., Brune, W. H., Miller, D. O., Blake, D., Long, R., Wisthaler, A., et al. (2017). Higher measured than modeled ozone production at increased NO_x levels in the Colorado Front Range. *Atmospheric Chemistry and Physics*, 17, 11273–11292. <https://doi.org/10.5194/acp-17-11273-2017>
- Baker, A. K., Beyersdorf, A. J., Doezeza, L. A., Katzenstein, A., Meinardi, S., Simpson, I. J., et al. (2008). Measurements of nonmethane hydrocarbons in 28 United States cities. *Atmospheric Environment*, 42, 170–182. <https://doi.org/10.1016/j.atmosenv.2007.09.007>
- Barletta, B., Meinardi, S., Sherwood Rowland, F., Chan, C.-Y., Wang, X., Zou, S., et al. (2005). Volatile organic compounds in 43 Chinese cities. *Atmospheric Environment*, 39, 5979–5990. <https://doi.org/10.1016/j.atmosenv.2005.06.029>
- Bien, T., & Helmig, D. (2018). Changes in summertime ozone in Colorado during 2000–2015. *Elementa: Science of the Anthropocene*, 6, 55. <https://doi.org/10.1525/elementa.300>
- Borbon, A., Gilman, J. B., Kuster, W. C., Grand, N., Chevaillier, S., Colomb, A., et al. (2013). Emission ratios of anthropogenic volatile organic compounds in northern mid-latitude megacities: Observations versus emission inventories in Los Angeles and Paris. *Journal of Geophysical Research: Atmospheres*, 118, 2041–2057. <https://doi.org/10.1002/jgrd.50059>
- Brown, S. S., Thornton, J. A., Keene, W. C., Pszenny, A. A. P., Sive, B. C., Dubé, W. P., et al. (2013). Nitrogen, Aerosol Composition, and Halogens on a Tall Tower (NACHTT): Overview of a wintertime air chemistry field study in the front range urban corridor of Colorado. *Journal of Geophysical Research: Atmospheres*, 118, 8067–8085. <https://doi.org/10.1002/jgrd.50537>
- Cazorla, M., Brune, W. H., Ren, X., & Lefer, B. (2012). Direct measurement of ozone production rates in Houston in 2009 and comparison with two estimation methods. *Atmospheric Chemistry and Physics*, 12, 1203–1212. <https://doi.org/10.5194/acp-12-1203-2012>

- Chen, T., Xue, L., Zheng, P., Zhang, Y., Liu, Y., Sun, J., et al. (2020). Volatile organic compounds and ozone air pollution in an oil production region in northern China. *Atmospheric Chemistry and Physics*, 20, 7069–7086. <https://doi.org/10.5194/acp-20-7069-2020>
- CNEMC. (2018). *Monthly report on air quality of China cities*. China National Environmental Monitoring Centre. Retrieved from <http://www.cnemc.cn/jcwg/kqzlkzkg/201808/P020181010529659662339.pdf>
- Crutzen, P. J., & Andreae, M. O. (1990). Biomass burning in the tropics: Impact on atmospheric chemistry and biogeochemical cycles. *Science*, 250(4988), 1669–1678. <https://doi.org/10.1126/science.250.4988.1669>
- Daum, P. H., Kleinman, L. I., Springston, S. R., Nunnermacker, L. J., Lee, Y.-N., Weinstein-Lloyd, J., et al. (2003). A comparative study of O₃ formation in the Houston urban and industrial plumes during the 2000 Texas Air Quality Study. *Journal of Geophysical Research*, 108(D23), 4715. <https://doi.org/10.1029/2003JD003552>
- de Gouw, J. A., Gilman, J. B., Kim, S.-W., Alvarez, S. L., Dusanter, S., Graus, M., et al. (2018). Chemistry of volatile organic compounds in the Los Angeles Basin: Formation of oxygenated compounds and determination of emission ratios. *Journal of Geophysical Research: Atmospheres*, 123, 2298–2319. <https://doi.org/10.1002/2017JD027976>
- de Gouw, J. A., Gilman, J. B., Kim, S. W., Lerner, B. M., Isaacman-VanWertz, G., McDonald, B. C., et al. (2017). Chemistry of volatile organic compounds in the Los Angeles Basin: Nighttime removal of alkenes and determination of emission ratios. *Journal of Geophysical Research: Atmospheres*, 122(11), 11843–11861. <https://doi.org/10.1002/2017JD027459>
- de Gouw, J. A., Middlebrook, A. M., Warneke, C., Goldan, P. D., Kuster, W. C., Roberts, J. M., et al. (2005). Budget of organic carbon in a polluted atmosphere: Results from the New England Air Quality Study in 2002. *Journal of Geophysical Research*, 110, D16305. <https://doi.org/10.1029/2004JD005623>
- DeCarlo, P. F., Kimmel, J. R., Trimborn, A., Northway, M. J., Jayne, J. T., Aiken, A. C., et al. (2006). Field-deployable, high-resolution, time-of-flight aerosol mass spectrometer. *Analytical Chemistry*, 78, 8281–8289. <https://doi.org/10.1021/Ac061249n>
- Decker, Z. C. J., Zarzana, K. J., Coggon, M., Min, K.-E., Pollack, I., Ryerson, T. B., et al. (2019). Nighttime chemical transformation in biomass burning plumes: A box model analysis initialized with aircraft observations. *Environmental Science & Technology*, 53(5), 2529–2538. <https://doi.org/10.1021/acs.est.8b05359>
- Dix, B., de Bruin, J., Roosenbrand, E., Vlemmix, T., Francoeur, C., Gorchov-Negron, A., et al. (2020). Nitrogen oxide emissions from U.S. oil and gas production: Recent trends and source attribution. *Geophysical Research Letters*, 47, e2019GL085866. <https://doi.org/10.1029/2019GL085866>
- Duncan, B. N., Lamsal, L. N., Thompson, A. M., Yoshida, Y., Lu, Z., Streets, D. G., et al. (2016). A space-based, high-resolution view of notable changes in urban NO_x pollution around the world (2005–2014). *Journal of Geophysical Research: Atmospheres*, 121, 976–996. <https://doi.org/10.1002/2015JD024121>
- Dunlea, E. J., Herndon, S. C., Nelson, D. D., Volkamer, R. M., San Martini, F., Sheehy, P. M., et al. (2007). Evaluation of nitrogen dioxide chemiluminescence monitors in a polluted urban environment. *Atmospheric Chemistry and Physics*, 7(10), 2691–2704. <https://doi.org/10.5194/acp-7-2691-2007>
- Edwards, P. M., Young, C. J., Aikin, K., de Gouw, J., Dubé, W. P., Geiger, F., et al. (2013). Ozone photochemistry in an oil and natural gas extraction region during winter: Simulations of a snow-free season in the Uintah Basin, Utah. *Atmospheric Chemistry and Physics*, 13(17), 8955–8971. <https://doi.org/10.5194/acp-13-8955-2013>
- EIA. (2015). *International analysis: China, technical report*.
- EIA. (2020). *Country analysis executive summary: China, technical report*. Energy Information Administration.
- Fischer, E. V., Jacob, D. J., Yantosca, R. M., Sulprizio, M. P., Millet, D. B., Mao, J. F., et al. (2014). Atmospheric peroxyacetyl nitrate (PAN): A global budget and source attribution. *Atmospheric Chemistry and Physics*, 14, 2679–2698. <https://doi.org/10.5194/acp-14-2679-2014>
- Fu, T.-M., Daniel, J. J., Paul, I. P., Kelly, C., Yuxuan, X. W., Barbara, B., et al. (2007). Space-based formaldehyde measurements as constraints on volatile organic compound emissions in east and south Asia and implications for ozone. *Journal of Geophysical Research*, 112, D06312. <https://doi.org/10.1029/2006jd007853>
- Fung, K., & Grosjean, D. (1985). Peroxybenzoyl nitrate: Measurements in smog chambers and in urban air. *Science of the Total Environment*, 46, 29–40. [https://doi.org/10.1016/0048-9697\(85\)90281-5](https://doi.org/10.1016/0048-9697(85)90281-5)
- Ge, B., Sun, Y., Liu, Y., Dong, H., Ji, D., Jiang, Q., et al. (2013). Nitrogen dioxide measurement by cavity attenuated phase shift spectroscopy (CAPS) and implications in ozone production efficiency and nitrate formation in Beijing, China. *Journal of Geophysical Research: Atmospheres*, 118, 9499–9509. <https://doi.org/10.1002/jgrd.50757>
- Gentner, D. R., Worton, D. R., Isaacman, G., Davis, L. C., Dallmann, T. R., Wood, E. C., et al. (2013). Chemical composition of gas-phase organic carbon emissions from motor vehicles and implications for ozone production. *Environmental Science & Technology*, 47(20), 11837–11848. <https://doi.org/10.1021/es401470e>
- Gilman, J. B., Kuster, W. C., Goldan, P. D., Herndon, S. C., Zahniser, M. S., Tucker, S. C., et al. (2009). Measurements of volatile organic compounds during the 2006 TexAQSGoMACCS campaign: Industrial influences, regional characteristics, and diurnal dependencies of the OH reactivity. *Journal of Geophysical Research*, 114, D00F06. <https://doi.org/10.1029/2008JD011525>
- Gilman, J. B., Lerner, B. M., Kuster, W. C., & de Gouw, J. A. (2013). Source signature of volatile organic compounds from oil and natural gas operations in northeastern Colorado. *Environmental Science & Technology*, 47(3), 1297–1305. <https://doi.org/10.1021/es304119a>
- Grosjean, E., Grosjean, D., Fraser, M. P., & Cass, G. R. (1996). Air quality model evaluation data for organics .3. Peroxyacetyl nitrate and peroxypropionyl nitrate in Los Angeles air. *Environmental Science & Technology*, 30, 2704–2714. <https://doi.org/10.1021/es9508535>
- Gu, D., Wang, Y., Smeltzer, C., & Liu, Z. (2013). Reduction in NO_x emission trends over China: Regional and seasonal variations. *Environmental Science & Technology*, 47(22), 12912–12919. <https://doi.org/10.1021/es401727e>
- Helmig, D. (2020). Air quality impacts from oil and natural gas development in Colorado. *Elementa: Science of the Anthropocene*, 8, 4. <https://doi.org/10.1525/elementa.398>
- Helmig, D., Thompson, C. R., Evans, J., Boylan, P., Hueber, J., & Park, J. H. (2014). Highly elevated atmospheric levels of volatile organic compounds in the Uintah Basin, Utah. *Environmental Science & Technology*, 48(9), 4707–4715. <https://doi.org/10.1021/es405046r>
- Ho, K. F., Lee, S. C., Ho, W. K., Blake, D. R., Cheng, Y., Li, Y. S., et al. (2009). Vehicular emission of volatile organic compounds (VOCs) from a tunnel study in Hong Kong. *Atmospheric Chemistry and Physics*, 9, 7491–7504. <https://doi.org/10.5194/acp-9-7491-2009>
- Huang, Y., Ling, Z. H., Lee, S. C., Ho, S. S. H., Cao, J. J., Blake, D. R., et al. (2015). Characterization of volatile organic compounds at a roadside environment in Hong Kong: An investigation of influences after air pollution control strategies. *Atmospheric Environment*, 122, 809–818. <https://doi.org/10.1016/j.atmosenv.2015.09.036>
- Jacob, D. J., Crawford, J. H., Kleb, M. M., Connors, V. S., Bendura, R. J., Raper, J. L., et al. (2003). Transport and Chemical Evolution over the Pacific (TRACE-P) aircraft mission: Design, execution, and first results. *Journal of Geophysical Research*, 108, 9000. <https://doi.org/10.1029/2002JD003276>

- Ji, Y., Huey, L. G., Tanner, D. J., Lee, Y. R., Veres, P. R., Neuman, J. A., et al. (2020). A vacuum ultraviolet ion source (VUV-IS) for iodide-chemical ionization mass spectrometry: A substitute for radioactive ion sources. *Atmos. Meas. Tech.*, *13*, 3683–3696. <https://doi.org/10.5194/amt-13-3683-2020>
- Kim, S., VandenBoer, T. C., Young, C. J., Riedel, T. P., Thornton, J. A., Swarthout, B., et al. (2014). The primary and recycling sources of OH during the NACHTT-2011 campaign: HONO as an important OH primary source in the wintertime. *Journal of Geophysical Research: Atmospheres*, *119*, 6886–6896. <https://doi.org/10.1002/2013JD019784>
- Kleffmann, J., Lörzer, J. C., Wiesen, P., Kern, C., Trick, S., Volkamer, R., et al. (2006). Intercomparison of the DOAS and LOPAP techniques for the detection of nitrous acid (HONO). *Atmospheric Environment*, *40*, 3640–3652. <https://doi.org/10.1016/j.atmosenv.2006.03.027>
- Kleinman, L. I., Daum, P. H., Imre, D. G., Lee, J. H., Lee, Y.-N., Nunnermacker, L. J., et al. (2000). Ozone production in the New York City Urban Plume. *Journal of Geophysical Research*, *105*, 14495–14511. <https://doi.org/10.1029/2000JD900011>
- Kleinman, L. I., Daum, P. H., Lee, Y. N., Nunnermacker, L. J., Springston, S. R., Weinstein-Lloyd, J., & Rudolph, J. (2002). Ozone production efficiency in an urban area. *Journal of Geophysical Research*, *107*, 4733. <https://doi.org/10.1029/2002jd002529>
- Koss, A. R., Sekimoto, K., Gilman, J. B., Selimovic, V., Coggon, M. M., Zarzana, K. J., et al. (2018). Non-methane organic gas emissions from biomass burning: Identification, quantification, and emission factors from PTR-ToF during the FIREX 2016 laboratory experiment. *Atmospheric Chemistry and Physics*, *18*, 3299–3319. <https://doi.org/10.5194/acp-18-3299-2018>
- Lai, C. H., Chang, C. C., Wang, C. H., Shao, M., Zhang, Y., & Wang, J. L. (2009). Emissions of liquefied petroleum gas (LPG) from motor vehicles. *Atmospheric Environment*, *43*, 1456–1463. <https://doi.org/10.1016/j.atmosenv.2008.11.045>
- Le, T., Wang, Y., Liu, L., Yang, J., Yung, Y. L., Li, G., & Seinfeld, J. H. (2020). Unexpected air pollution with marked emission reductions during the COVID-19 outbreak in China. *Science*, *369*, 702–706. <https://doi.org/10.1126/science.abb7431>
- Lee, G., Jang, Y., Lee, H., Han, J.-S., Kim, K.-R., & Lee, M. (2008). Characteristic behavior of peroxyacetyl nitrate (PAN) in Seoul megacity, Korea. *Chemosphere*, *73*(4), 619–628. <https://doi.org/10.1016/j.chemosphere.2008.05.060>
- Li, G., Bei, N., Cao, J., Wu, J., Long, X., Feng, T., et al. (2017). Widespread and persistent ozone pollution in eastern China during the non-winter season of 2015: Observations and source attributions. *Atmospheric Chemistry and Physics*, *17*, 2759–2774. <https://doi.org/10.5194/acp-17-2759-2017>
- Li, J., Hao, Y., Simayi, M., Shi, Y., Xi, Z., & Xie, S. (2019). Verification of anthropogenic VOC emission inventory through ambient measurements and satellite retrievals. *Atmospheric Chemistry and Physics*, *19*(9), 5905–5921. <https://doi.org/10.5194/acp-19-5905-2019>
- Li, J., Xie, S. D., Zeng, L. M., Li, L. Y., Li, Y. Q., & Wu, R. R. (2015). Characterization of ambient volatile organic compounds and their sources in Beijing, before, during, and after Asia-Pacific Economic Cooperation China 2014. *Atmospheric Chemistry and Physics*, *15*, 7945–7959. <https://doi.org/10.5194/acp-15-7945-2015>
- Li, K., Jacob, D. J., Liao, H., Shen, L., Zhang, Q., & Bates, K. H. (2019). Anthropogenic drivers of 2013–2017 trends in summer surface ozone in China. *Proceedings of the National Academy of Sciences of the United States of America*, *116*(2), 422–427. <https://doi.org/10.1073/pnas.1812168116>
- Li, K., Jacob, D. J., Shen, L., Lu, X., Smedt, I. D., & Liao, H. (2020). Increases in surface ozone pollution in China from 2013 to 2019: Anthropogenic and meteorological influences. *Atmospheric Chemistry and Physics*, *20*, 11423–11433. <https://doi.org/10.5194/acp-20-11423-2020>
- Liao, J., Huey, L. G., Liu, Z., Tanner, D. J., Cantrell, C. A., Orlando, J. J., et al. (2014). High levels of molecular chlorine in the Arctic atmosphere. *Nature Geoscience*, *7*(2), 91–94. <https://doi.org/10.1038/ngeo2046>
- Lindaas, J., Farmer, D. K., Pollack, I. B., Abeleira, A., Flocke, F., & Fischer, E. V. (2019). Acyl peroxy nitrates link oil and natural gas emissions to high ozone abundances in the Colorado front range during summer 2015. *Journal of Geophysical Research: Atmospheres*, *124*, 2336–2350. <https://doi.org/10.1029/2018jd028825>
- Liu, C., Ma, Z., Mu, Y., Liu, J., Zhang, C., Zhang, Y., et al. (2017). The levels, variation characteristics, and sources of atmospheric non-methane hydrocarbon compounds during wintertime in Beijing, China. *Atmospheric Chemistry and Physics*, *17*, 10633–10649. <https://doi.org/10.5194/acp-17-10633-2017>
- Liu, J. P., Li, S., Mekic, M., Jiang, H. Y., Zhou, W. T., Loisel, G., et al. (2019). Photoenhanced uptake of NO₂ and HONO formation on real urban grime. *Environmental Science and Technology Letters*, *6*, 413–417. <https://doi.org/10.1021/acs.estlett.9b00308>
- Liu, X., Huey, L. G., Yokelson, R. J., Selimovic, V., Simpson, I. J., Müller, M., et al. (2017). Airborne measurements of western U.S. wildfire emissions: Comparison with prescribed burning and air quality implications. *Journal of Geophysical Research: Atmospheres*, *122*, 6108–6129. <https://doi.org/10.1002/2016JD026315>
- Liu, X., Zhang, Y., Huey, L. G., Yokelson, R. J., Wang, Y., Jimenez, J. L., et al. (2016). Agricultural fires in the southeastern U.S. during SEA-C4RS: Emissions of trace gases and particles and evolution of ozone, reactive nitrogen, and organic aerosol. *Journal of Geophysical Research: Atmospheres*, *121*, 7383–7414. <https://doi.org/10.1002/2016JD025040>
- Liu, Z., Wang, Y., Gu, D., Zhao, C., Huey, L. G., Stickel, R., et al. (2010). Evidence of reactive aromatics as a major source of peroxy acetyl nitrate over China. *Environmental Science & Technology*, *44*, 7017–7022. <https://doi.org/10.1021/es1007966>
- Liu, Z., Wang, Y., Gu, D., Zhao, C., Huey, L. G., Stickel, R., et al. (2012). Summertime photochemistry during CAREBeijing-2007: RO_x budgets and O₃ formation. *Atmospheric Chemistry and Physics*, *12*(16), 7737–7752. <https://doi.org/10.5194/acp-12-7737-2012>
- Lough, G. C., Schauer, J. J., Lonneman, W. A., & Allen, M. K. (2005). Summer and winter nonmethane hydrocarbon emissions from on-road motor vehicles in the midwestern United States. *Journal of the Air & Waste Management Association (1995)*, *55*, 629–646. <https://doi.org/10.1080/10473289.2005.10464649>
- Lu, X., Guo, H., Boyd, C. M., Klein, M., Bougiatioti, A., Cerully, K. M., et al. (2015). Effects of anthropogenic emissions on aerosol formation from isoprene and monoterpenes in the southeastern United States. *Proceedings of the National Academy of Sciences of the United States of America*, *112*(1), 37–42. <https://doi.org/10.1073/pnas.1417609112>
- Lyu, X., Guo, H., Simpson, I. J., Meinardi, S., Louie, P. K. K., Ling, Z. H., et al. (2016). Effectiveness of replacing catalytic converters in LPG-fueled vehicles in Hong Kong. *Atmospheric Chemistry and Physics*, *16*, 6609–6626. <https://doi.org/10.5194/acp-16-6609-2016>
- Ma, M., Gao, Y., Wang, Y., Zhang, S., Leung, L. R., Liu, C., et al. (2019). Substantial ozone enhancement over the North China Plain from increased biogenic emissions due to heat waves and land cover in summer 2017. *Atmospheric Chemistry and Physics*, *19*(19), 12207–12195. <https://doi.org/10.5194/acp-19-12195-2019>
- May, A. A., Nguyen, N. T., Presto, A. A., Gordon, T. D., Lipsky, E. M., Karve, M., et al. (2014). Gas- and particle-phase primary emissions from in-use, on-road gasoline and diesel vehicles. *Atmospheric Environment*, *88*, 247–260. <https://doi.org/10.1016/j.atmosenv.2014.01.046>
- McDonald, B. C., de Gouw, J. A., Gilman, J. B., Jathar, S. H., Akherati, A., Cappa, C. D., et al. (2018). Volatile chemical products emerging as largest petrochemical source of urban organic emissions. *Science*, *359*(6377), 760–764. <https://doi.org/10.1126/science.aag0524>
- McDuffie, E. E., Edwards, P. M., Gilman, J. B., Lerner, B. M., Dubé, W. P., Trainer, M., et al. (2016). Influence of oil and gas emissions on summertime ozone in the Colorado Northern Front Range. *Journal of Geophysical Research: Atmospheres*, *121*, 8712–8729. <https://doi.org/10.1002/2016JD025265>

- McKeen, S. A., & Liu, S. C. (1993). Hydrocarbon ratios and photochemical history of air masses. *Geophysical Research Letters*, *20*, 2363–2366. <https://doi.org/10.1029/93gl02527>
- Meijer, G. M., & Nieboer, H. (1977). *VDI Ber. (Ver. D&h. Ing.)* (pp. 55–56). [https://doi.org/10.1016/0304-3479\(77\)90020-5](https://doi.org/10.1016/0304-3479(77)90020-5)
- Monks, P. S., Rickard, A. R., & Hall, S. L. (2004). Attenuation of spectral actinic flux and photolysis frequencies at the surface through homogeneous cloud fields. *Journal of Geophysical Research*, *109*. <https://doi.org/10.1029/2003jd004076>
- Nault, B. A., Schroder, J. C., Campuzano-Jost, P., Day, D. A., Anderson, B., Beyersdorf, A. J., et al. (2018). Secondary organic aerosol production from local emissions dominates the organic aerosol budget over Seoul, South Korea, during KORUS-AQ. *Atmospheric Chemistry and Physics*, *18*, 17769–17800. <https://doi.org/10.5194/acp-18-17769-2018>
- Ou, J. M., Guo, H., Zheng, J. Y., Cheung, K., Louie, P. K. K., Ling, Z. H., & Wang, D. W. (2015). Concentrations and sources of nonmethane hydrocarbons (NMHCs) from 2005 to 2013 in Hong Kong: A multi-year real-time data analysis. *Atmospheric Environment*, *103*, 196–206. <https://doi.org/10.1016/j.atmosenv.2014.12.048>
- Parrish, D. D., Stohl, A., Forster, C., Atlas, E. L., Blake, D. R., Goldan, P. D., et al. (2007). Effects of mixing on evolution of hydrocarbon ratios in the troposphere. *Journal of Geophysical Research*, *112*, D10S34. <https://doi.org/10.1029/2006JD007583>
- Peischl, J., Eilerman, S. J., Neuman, J. A., Aikin, K. C., de Gouw, J., Gilman, J. B., et al. (2018). Quantifying methane and ethane emissions to the atmosphere from central and western U.S. oil and natural gas production regions. *Journal of Geophysical Research: Atmospheres*, *123*, 7725–7740. <https://doi.org/10.1029/2018JD028622>
- Peischl, J., Ryerson, T., Brioude, J., Aikin, K., Andrews, A., Atlas, E. L., et al. (2013). Quantifying sources of methane using light alkanes in the Los Angeles basin, California. *Journal of Geophysical Research: Atmospheres*, *118*, 4974–4990. <https://doi.org/10.1002/jgrd.50413>
- Perring, A. E., Pusede, S. E., & Cohen, R. C. (2013). An observational perspective on the atmospheric impacts of alkyl and multifunctional nitrates on ozone and secondary organic aerosol. *Chemical Reviews*, *113*, 5848–5870. <https://doi.org/10.1021/cr300520x>
- Pétron, G., Frost, G., Miller, B. R., Hirsch, A. I., Montzka, S. A., Karion, A., et al. (2012). Hydrocarbon emissions characterization 1021 in the Colorado Front Range: A pilot study. *Journal of Geophysical Research*, *117*, D04304. <https://doi.org/10.1029/2011JD016360>
- Pétron, G., Karion, A., Sweeney, C., Miller, B. R., Montzka, S. A., Frost, G. J., et al. (2014). A new look at methane and nonmethane hydrocarbon emissions from oil and natural gas operations in the Colorado Denver- Julesburg Basin. *Journal of Geophysical Research: Atmospheres*, *119*, 6836–6852. <https://doi.org/10.1002/2013jd021272>
- Qiu, Y., Ma, Z., Li, K., Lin, W., Tang, Y., Dong, F., & Liao, H. (2020). Markedly enhanced levels of peroxyacetyl nitrate (PAN) during COVID-19 in Beijing. *Geophysical Research Letters*, *47*, e2020GL089623. <https://doi.org/10.1029/2020GL089623>
- Qu, H., Wang, Y., Zhang, R., & Li, J. (2020). Extending ozone-precursor relationships in China from peak concentration to peak time. *Journal of Geophysical Research*, *125*, e2020JD033670. <https://doi.org/10.1029/2020JD033670>
- Roberts, J. M. (2007). PAN and related compounds. In *Volatile organic compounds in the atmosphere* (pp. 221–268). Blackwell Publishing Ltd. <https://doi.org/10.1002/9780470988657.ch6>
- Roberts, J. M., Flocke, F., Chen, G., de Gouw, J., Holloway, J. S., Hübler, G., et al. (2004). Measurement of peroxyacetic nitric anhydrides (PANs) during the ITCT 2K2 aircraft intensive experiment. *Journal of Geophysical Research*, *109*, D23S21. <https://doi.org/10.1029/2004JD004960>
- Roberts, J. M., Flocke, F., Stroud, C. A., Hereid, D., Williams, E., Fehsenfeld, F., et al. (2002). Ground-based measurements of peroxyacetic nitric anhydrides (PANs) during the 1999 Southern Oxidants Study Nashville Intensive. *Journal of Geophysical Research*, *107*(D21), 4554. <https://doi.org/10.1029/2001JD000947>
- Roberts, J. M., Flocke, F., Weinheimer, A., Tamimoto, H., Jobson, B. T., Riemer, D., et al. (2001). Observations of APAN during TexAQs 2000. *Geophysical Research Letters*, *28*, 4195–4198. <https://doi.org/10.1029/2001GL013466>
- Roberts, J. M., Jobson, B. T., Kuster, W., Goldan, P., Murphy, P., Williams, E., et al. (2003). An examination of the chemistry of peroxyacetic nitric anhydrides and related volatile organic compounds during Texas Air Quality Study 2000 using ground-based measurements. *Journal of Geophysical Research*, *108*(D16), 4495. <https://doi.org/10.1029/2003JD003383>
- Ryerson, T. B., Trainer, M., Angevine, W. M., Brock, C. A., Dissly, R. W., Fehsenfeld, F. C., et al. (2003). Effect of petrochemical industrial emissions of reactive alkenes and NO_x on tropospheric ozone formation in Houston, Texas. *Journal of Geophysical Research*, *108*(D8), 4249. <https://doi.org/10.1029/2002JD003070>
- Schroeder, J. R., Crawford, J. H., Ahn, J.-Y., Chang, L., Fried, A., Walega, J., et al. (2020). Observation-based modeling of ozone chemistry in the Seoul metropolitan area during the Korea-United States Air Quality Study (KORUS-AQ). *Elementa*, *8*, 3. <https://doi.org/10.1525/elementa.400>
- Seinfeld, J. H., & Pandis, S. N. (2016). *Atmospheric chemistry and physics: From air pollution to climate change* (3rd ed.). John Wiley & Sons, Inc.
- Shetter, R. E., & Müller, M. (1999). Photolysis frequency measurements using actinic flux spectroradiometry during the PEM-Tropics mission: Instrumentation description and some results. *Journal of Geophysical Research: Atmospheres*, *104*(D5), 5647–5661. <https://doi.org/10.1029/98jd01381>
- Sillman, S., Logan, J. A., & Wofsy, S. C. (1990). The sensitivity of ozone to nitrogen oxides and hydrocarbons in regional ozone episodes. *Journal of Geophysical Research*, *95*, 1837–1851. <https://doi.org/10.1029/JD095iD02p01837>
- Simpson, I. J. (2020). Characterization, sources and reactivity of volatile organic compounds (VOCs) in Seoul and surrounding regions during KORUS-AQ. *Elementa: Science of the Anthropocene*, *8*, 37. <https://doi.org/10.1525/elementa.434>
- Slusher, D. L., Huey, L. G., Tanner, D. J., Flocke, F. M., & Roberts, J. M. (2004). A thermal dissociation-chemical ionization mass spectrometry (TD-CIMS) technique for the simultaneous measurement of peroxyacetyl nitrates and dinitrogen pentoxide. *Journal of Geophysical Research*, *109*, D19315. <https://doi.org/10.1029/2004JD004670>
- Sprengnether, M. M., Demerjian, K. L., Dransfield, T. J., Clarke, J. S., Anderson, J. G., & Donahue, N. M. (2009). Rate constants of nine C₆-C₉ alkanes with OH from 230 to 379 K: Chemical tracers for [OH]. *Journal of Physical Chemistry*, *113*(17), 5030–5038. <https://doi.org/10.1021/jp810412m>
- Swarthout, R. F., Russo, R. S., Zhou, Y., Hart, A. H., & Sive, B. C. (2013). Volatile organic compound distributions during the NACHTT campaign at the Boulder Atmospheric Observatory: Influence of urban and natural gas sources. *Journal of Geophysical Research: Atmospheres*, *118*(10), 10614–10637. <https://doi.org/10.1002/jgrd.50722>
- Talbot, R., Dibb, J., Scheuer, E., Seid, G., Russo, R., Sandholm, S., et al. (2003). Reactive nitrogen in Asian continental outflow over the western Pacific: Results from the NASA Transport and Chemical Evolution over the Pacific (TRACE-P) airborne mission. *Journal of Geophysical Research*, *108*(D20), 8803. <https://doi.org/10.1029/2002JD003129>
- Tan, Z., Fuchs, H., Lu, K., Hofzumahaus, A., Bohn, B., Broch, S., et al. (2017). Radical chemistry at a rural site (Wangdu) in the North China Plain: Observation and model calculations of OH, HO₂ and RO₂ radicals. *Atmospheric Chemistry and Physics*, *17*, 663–690. <https://doi.org/10.5194/acp-17-663-2017>

- Tan, Z., Lu, K., Hofzumahaus, A., Fuchs, H., Bohn, B., Holland, F., et al. (2019). Experimental budgets of OH, HO₂, and RO₂ radicals and implications for ozone formation in the Pearl River Delta in China 2014. *Atmospheric Chemistry and Physics*, *19*, 7129–7150. <https://doi.org/10.5194/acp-19-7129-2019>
- Tan, Z., Lu, K., Hofzumahaus, A., Fuchs, H., Bohn, B., Holland, F., et al. (2020). No evidence for a significant impact of heterogeneous chemistry on radical concentrations in the North China Plain in summer 2014. *Environmental Science & Technology*, *54*, 5973–5979. <https://doi.org/10.1021/acs.est.0c00525>
- Tan, Z., Lu, K., Jiang, M., Su, R., Wang, H., Lou, S., et al. (2019). Daytime atmospheric oxidation capacity in four Chinese megacities during the photochemically polluted season: A case study based on box model simulation. *Atmospheric Chemistry and Physics*, *19*, 3493–3513. <https://doi.org/10.5194/acp-19-3493-2019>
- Tan, Z., Rohrer, F., Lu, K. D., Ma, X. F., Bohn, B., Broch, S., et al. (2018). Wintertime photochemistry in Beijing: Observations of RO_x radical concentrations in the North China Plain during the BEST-ONE campaign. *Atmospheric Chemistry and Physics*, *18*, 12391–12411. <https://doi.org/10.5194/acp-18-12391-2018>
- Tanimoto, A., & Akimoto, H. (2001). A new peroxy-carboxylic nitric anhydride identified in the atmosphere: CH₂=CHC(O)OONO₂ (APAN). *Geophysical Research Letters*, *28*, 2831–2834. <https://doi.org/10.1029/2001GL012998>
- Tanimoto, H., Hirokawa, J., Kajii, Y., & Akimoto, H. (1999). A new measurement technique of peroxyacetyl nitrate at parts per trillion by volume levels: Gas chromatography/negative ion chemical ionization mass spectrometry. *Journal of Geophysical Research*, *104*, 21343–21354. <https://doi.org/10.1029/1999jd900345>
- Thompson, C. R., Hueber, J., & Helmig, D. (2014). Influence of oil and gas emissions on ambient atmospheric non-methane hydrocarbons in residential areas of Northeastern Colorado. *Elementa: Science of the Anthropocene*, *2*, 000035. <https://doi.org/10.12952/journal.elementa.000035>
- Toma, S., Bertman, S., Groff, C., Xiong, F., Shepson, P. B., Romer, P., et al. (2019). Importance of biogenic volatile organic compounds to acyl peroxy nitrates (APN) production in the southeastern US during SOAS 2013. *Atmospheric Chemistry and Physics*, *19*, 1867–1880. <https://doi.org/10.5194/acp-19-1867-2019>
- Tsai, W. Y., Chan, L. Y., Blake, D. R., & Chu, K. W. (2006). Vehicular fuel composition and atmospheric emissions in South China: Hong Kong, Macau, Guangzhou, and Zhuhai. *Atmospheric Chemistry and Physics*, *6*, 3281–3288. <https://doi.org/10.5194/acp-6-3281-2006>
- Wang, M., Shao, M., Chen, W., Lu, S., Liu, Y., Yuan, B., et al. (2015). Trends of non-methane hydrocarbons (NMHC) emissions in Beijing during 2002–2013. *Atmospheric Chemistry and Physics*, *15*, 1489–1502. <https://doi.org/10.5194/acp-15-1489-2015>
- Wang, M., Shao, M., Chen, W., Yuan, B., Lu, S., Zhang, Q., et al. (2014). A temporally and spatially resolved validation of emission inventories by measurements of ambient volatile organic compounds in Beijing, China. *Atmospheric Chemistry and Physics*, *14*, 5871–5891. <https://doi.org/10.5194/acp-14-5871-2014>
- Wang, T., Nie, W., Gao, J., Xue, L. K., Gao, X. M., Wang, X. F., et al. (2010). Air quality during the 2008 Beijing Olympics: Secondary pollutants and regional impact. *Atmospheric Chemistry and Physics*, *10*, 7603–7615. <https://doi.org/10.5194/acp-10-7603-2010>
- Wang, T., Xue, L., Brimblecombe, P., Lam, Y. F., Li, L., & Zhang, L. (2017). Ozone pollution in China: A review of concentrations, meteorological influences, chemical precursors, and effects. *The Science of the Total Environment*, *575*, 1582–1596. <https://doi.org/10.1016/j.scitotenv.2016.10.081>
- Wang, X., Liu, T., Bernard, F., Ding, X., Wen, S., Zhang, Y., et al. (2014). Design and characterization of a smog chamber for studying gas-phase chemical mechanisms and aerosol formation. *Atmospheric Measurement Techniques*, *7*, 301–313. <https://doi.org/10.5194/amt-7-301-2014>
- Wang, Y. H., Choi, Y. S., Zeng, T., Ridley, B., Blake, N., Blake, D., & Flocke, F. (2006). Late-spring increase of trans-Pacific pollution transport in the upper troposphere. *Geophysical Research Letters*, *33*, L01811. <https://doi.org/10.1029/2005GL024975>
- Warneke, C., Geiger, F., Edwards, P. M., Dube, W., Pétron, G., Kofler, J., et al. (2014). Volatile organic compound emissions from the oil and natural gas industry in the Uintah Basin, Utah: Oil and gas well pad emissions compared to ambient air composition. *Atmospheric Chemistry and Physics*, *14*(20977–10), 10988. <https://doi.org/10.5194/acp-14-10977-2014>
- Warneke, C., McKeen, S. A., de Gouw, J. A., Goldan, P. D., Kuster, W. C., Holloway, J. S., et al. (2007). Determination of urban volatile organic compound emission ratios and comparison with an emissions database. *Journal of Geophysical Research*, *112*, D10S47. <https://doi.org/10.1029/2006JD007930>
- Washenfelder, R. A., Trainer, M., Frost, G. J., Ryerson, T. B., Atlas, E. L., de Gouw, J. A., et al. (2010). Characterization of NO_x, SO₂, ethene, and propene from industrial emission sources in Houston, Texas. *Journal of Geophysical Research*, *115*, D16311. <https://doi.org/10.1029/2009JD013645>
- Wennberg, P. O., Mui, W., Wunch, D., Kort, E. A., Blake, D. R., Atlas, E. L., et al. (2012). On the sources of methane to the Los Angeles atmosphere. *Environmental Science & Technology*, *46*(17), 9282–9289. <https://doi.org/10.1021/es301138y>
- Wert, B. P., Trainer, M., Fried, A., Ryerson, T. B., Henry, B., Potter, W., et al. (2003). Signatures of terminal alkene oxidation in airborne formaldehyde measurements during TexAQS 2000. *Journal of Geophysical Research*, *108*(D3), 4104. <https://doi.org/10.1029/2002JD002502>
- Wilson, E. W., Hamilton, W. A., Kennington, H. R., Evans, B., Scott, N. W., & Demore, W. B. (2006). Measurement and estimation of rate constants for the reactions of hydroxyl radical with several alkanes and cycloalkanes. *The Journal of Physical Chemistry A*, *110*, 3593–3604. <https://doi.org/10.1021/jp055841c>
- Winer, A. M., Peters, J. W., Smith, J. P., & Pitts, J. N., Jr (1974). Response of commercial chemiluminescent nitric oxide-nitrogen dioxide analyzers to other nitrogen-containing compounds. *Environmental Science & Technology*, *8*, 1118–1121. <https://doi.org/10.1021/es60098a004>
- Wolfe, G. M., Cantrell, C., Kim, S., Mauldin, R. L., Karl, T., Harley, P., et al. (2014). Missing peroxy radical sources within a summertime ponderosa pine forest. *Atmospheric Chemistry and Physics*, *14*, 4715–4732. <https://doi.org/10.5194/acp-14-4715-2014>
- Wolfe, G. M., Marvin, M. R., Roberts, S. J., Travis, K. R., & Liao, J. (2016). The Framework for 0-D Atmospheric Modeling (FOAM) v3.1. *Geoscientific Model Development*, *9*, 3309–3319. <https://doi.org/10.5194/gmd-9-3309-2016>
- Wu, C., & Yu, J. Z. (2018). Evaluation of linear regression of techniques for atmospheric applications: The importance of appropriate weighting. *Atmospheric Measurement Techniques*, *11*, 1233–1250. <https://doi.org/10.5194/amt-11-1233-2018>
- Wu, R., & Xie, S. (2017). Spatial distribution of ozone formation in China derived from emissions of speciated volatile organic compounds. *Environmental Science & Technology*, *51*, 2574–2583. <https://doi.org/10.1021/acs.est.6b03634>
- Yokelson, R. J., Crouse, J. D., DeCarlo, P. F., Karl, T., Urbanski, S., Atlas, E., et al. (2009). Emissions from biomass burning in the Yucatan. *Atmospheric Chemistry and Physics*, *9*(15), 5785–5812. <https://doi.org/10.5194/acp-9-5785-2009>
- Yuan, B., Hu, W., Shao, M., Wang, M., Chen, W. T., Lu, S. H., et al. (2013). VOC emissions, evolutions and contributions to SOA formation at a receptor site in eastern China. *Atmospheric Chemistry and Physics*, *13*, 8815–8832. <https://doi.org/10.5194/acp-13-8815-2013>
- Yuan, B., Shao, M., de Gouw, J. A., Parrish, D. D., Lu, S., Wang, M., et al. (2012). Volatile organic compounds (VOCs) in urban air: How chemistry affects the interpretation of positive matrix factorization (PMF) analysis. *Journal of Geophysical Research*, *117*, D24302. <https://doi.org/10.1029/2012JD018236>

- Zaragoza, J., Callahan, S., McDuffie, E. E., Kirkland, J., Brophy, P., Durrett, L., & Fischer, E. V. (2017). Observations of acyl peroxy nitrates during the Front Range Air Pollution and Photochemistry Experiment (FRAPPÉ). *Journal of Geophysical Research: Atmospheres*, *122*(12), 12416–12432. <https://doi.org/10.1002/2017jd027337>
- Zhang, B., Zhao, X., & Zhang, J. (2019). Characteristics of peroxyacetyl nitrate pollution during a 2015 winter haze episode in Beijing. *Environmental Pollution*, *244*, 379–387. <https://doi.org/10.1016/j.envpol.2018.10.078>
- Zhang, G., Xia, L., Zang, K., Xu, W., Zhang, F., Liang, L., et al. (2020). The abundance and inter-relationship of atmospheric peroxyacetyl nitrate (PAN), peroxypropionyl nitrate (PPN), O₃, and NO_y during the wintertime in Beijing, China. *The Science of the Total Environment*, *718*, 137388. <https://doi.org/10.1016/j.scitotenv.2020.137388>
- Zhang, Y., Sun, J., Zheng, P., Chen, T., Liu, Y., Han, G., et al. (2019). Observations of C1–C5 alkyl nitrates in the Yellow River Delta, northern China: Effects of biomass burning and oil field emissions. *The Science of the Total Environment*, *656*, 129–139. <https://doi.org/10.1016/j.scitotenv.2018.11.208>
- Zhang, Y., Zhang, R., Yu, J., Zhang, Z., Yang, W., Zhang, H., et al. (2020). Isoprene mixing ratios measured at twenty sites in China during 2012–2014: Comparison with model simulation. *Journal of Geophysical Research: Atmospheres*, *125*, e2020JD033523. <https://doi.org/10.1029/2020JD033523>
- Zhang, Z., Zhang, Y., Wang, X., Lü, S., Huang, Z., Huang, X., et al. (2016). Spatiotemporal patterns and source implications of aromatic hydrocarbons at six rural sites across China's developed coastal regions. *Journal of Geophysical Research: Atmospheres*, *121*, 6669–6687. <https://doi.org/10.1002/2016JD025115>
- Zheng, W., Flocke, F. M., Tyndall, G. S., Swanson, A., Orlando, J. J., Roberts, J. M., et al. (2011). Characterization of a thermal decomposition chemical ionization mass spectrometer for the measurement of peroxy acyl nitrates (PANs) in the atmosphere. *Atmospheric Chemistry and Physics*, *11*, 6529–6547. <https://doi.org/10.5194/acp-11-6529-2011>
- Zhou, W., Cohan, D. S., & Henderson, B. H. (2014). Slower ozone production in Houston, Texas following emission reductions: Evidence from Texas Air Quality Studies in 2000 and 2006. *Atmospheric Chemistry and Physics*, *14*, 2777–2788. <https://doi.org/10.5194/acp-14-2777-2014>